Title

An evolved AAV variant enables efficient genetic engineering of murine T cells

Permalink

https://escholarship.org/uc/item/7th4849j

Journal

Cell, 186(2)

ISSN

0092-8674

Authors

Nyberg, William A

Ark, Jonathan

To, Angela

et al.

Publication Date

2023

DOI

10.1016/j.cell.2022.12.022

Peer reviewed

An evolved AAV variant enables efficient genetic engineering of murine T cells

William A. Nyberg[1,2,*], **Jonathan Ark**[3,*], **Angela To**[1,2], **Sylvanie Clouden**[4], **Gabriella Reeder**[1,2,5], **Joseph J. Muldoon**[1,2], **Jing-Yi Chung**[1,2], **William H. Xie**[1,5], **Vincent Allain**[1,2,6], **Zachary Steinhart**[1,2], **Christopher Chang**[1,2,5,7], **Alexis Talbot**[1,2,6], **Sandy Kim**[8], **Alan Rosales**[9], **L. Patrick Havlik**[9], **Harold Pimentel**[8,10], **Aravind Asokan**[3,4,9], **Justin Eyquem**[1,2,11,12,13,14]

[1]Department of Medicine, University of California, San Francisco, San Francisco, CA 94143, USA

[2]Gladstone-UCSF Institute of Genomic Immunology, San Francisco, CA 94158, USA

[3]Department of Molecular Genetics & Microbiology, Duke University School of Medicine, Durham, NC 27710, USA

[4]Department of Surgery, Duke University School of Medicine, Durham, NC 27710, USA

[5]Biomedical Sciences Graduate Program, University of California, San Francisco, San Francisco 94131, CA, USA

[6]Université de Paris Cité, INSERM UMR976, Hôpital St-Louis, Paris, France

[7]Medical Scientist Training Program, University of California, San Francisco, San Francisco, CA 94131, USA

[8]Bioinformatics Interdepartmental Program, University of California, Los Angeles, Los Angeles, CA 90095, USA

[9]Department of Biomedical Engineering, Duke University, Durham, NC 27710, USA

[10]Howard Hughes Medical Institute, Sloan Foundation, Departments of Computational Medicine, Human Genetics, University of California, Los Angeles, Los Angeles, CA 90095, USA

[11]Parker Institute for Cancer Immunotherapy, San Francisco, CA 94143, USA

Correspondence to: justin.eyquem@ucsf.edu and aravind.asokan@duke.edu.
*These authors contributed equally

[12]Department of Microbiology and Immunology, University of California San Francisco, San Francisco, CA, USA

[13]UCSF Helen Diller Family Comprehensive Cancer Center, University of California San Francisco, San Francisco, CA, USA.

[14]Lead contact

SUMMARY

Precise targeting of large transgenes to T cells using homology-directed repair has been transformative for adoptive cell therapies and T cell biology. Delivery of DNA templates via adeno-associated virus (AAV) has greatly improved knock-in efficiencies, but the tropism of current AAV serotypes restricts their use to human T cells employed in immunodeficient mouse models. To enable targeted knock-ins in murine T cells, we evolved Ark313, a synthetic AAV that exhibits high transduction efficiency in murine T cells. We performed a genome-wide knockout screen and identified QA2 as an essential factor for Ark313 infection. We demonstrate that Ark313 can be used for nucleofection-free DNA delivery, CRISPR/Cas9-mediated knockouts, and targeted integration of large transgenes. Ark313 enables pre-clinical modeling of *Trac*-targeted CAR-T and transgenic TCR-T cells in immunocompetent models. Efficient gene targeting in murine T cells holds great potential for improved cell therapies and opens avenues in experimental T cell immunology.

In Brief:

By combining structure-guided evolution and genome-wide screening, this work to identifies an adeno-associated virus and co-factor that enable gene targeting at high efficiencies in mouse T lymphocytes, thus opening the path for T cell manipulations in murine models.

Graphical Abstract
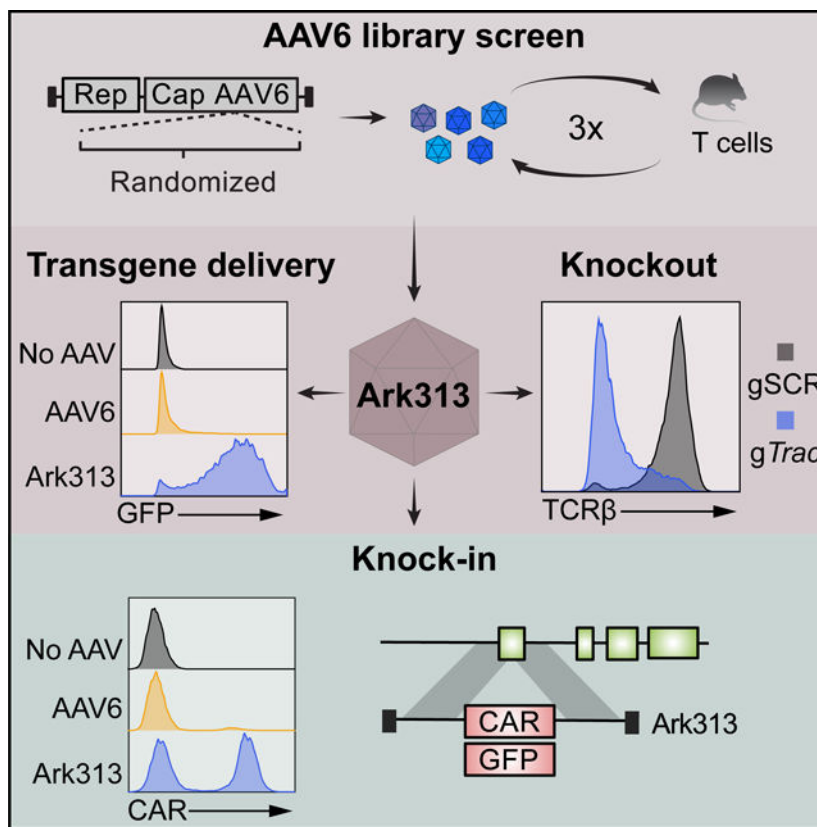
INTRODUCTION

Decades of research have placed T lymphocytes at the center of adaptive immunity and tolerance. Advances in the ability to engineer the T cell genome and modulate gene expression have been fundamental to our understanding of the regulation of T cell development and function in both health and disease. Recently, T cells engineered to express a chimeric antigen receptor (CAR) have been transformative in treating hematological malignancies[1,2], and there is great interest in extending this modality to the treatment of solid tumors[3]. The most common recombinant gene delivery vectors for T cells are replication-defective retroviruses such as γ-retroviruses (gRV) or lentiviruses, which result in semi-random integration and variable transgene expression due to variegation. Position effects can lead to heterogeneous T cell function, transgene silencing, and insertional oncogenesis, which limit the efficacy and safety of these therapeutic products[4,5].

Advances in gene editing technologies have enabled the precise integration of transgenes in primary human T cells[6,7] and broadened the scope of experimental and clinical T cell engineering strategies. We have shown that the targeted integration of a CAR at the TCRα constant (*TRAC*) locus under the control of the endogenous promoter confers physiologic receptor expression and yields T cells with superior anti-tumor activity compared to γ-retroviral delivery in xenograft mouse models. Gene targeting to the *TRAC* locus has also been reported to improve the activity of transgenic TCRs[8–10]. In a similar vein, we recently remodeled the TCR specificity to target cell-surface antigens in an HLA-independent

manner, and this HLA-independent TCR (HIT) benefited from the physiologic signal transduction and antigen sensitivity of the TCR locus and architecture[11].

In the context of T cells, only immunocompetent models can recapitulate the complexity of a tumor microenvironment or autoimmune niche. However, the identification of an efficient and non-toxic method for targeting large DNA cargo to murine T cells has remained elusive. Nucleofection of TALEN mRNA[12] or Cas9 ribonucleoprotein (RNP)[13] has been used to generate knockouts, but homology-directed repair template (HDRT) delivery has been a bottleneck for large knock-ins. HDRTs have been delivered to human T cells using adeno-associated virus serotype 6 (AAV6)[6,7] or DNA[8,14], with AAV6 remaining the more efficient and less toxic method. In contrast to human T cells, attempts to edit murine T cells by nucleofecting a short ssDNA or dsDNA HDRT (for making a single-nucleotide mutation) resulted in low targeting (<10%) and high toxicity (50–85% cell death)[15]. AAV could potentially solve these issues, but to date there is no AAV serotype that can transduce murine T cells with high efficiency, and thus there is a crucial unmet need for AAV variants with this tropism. To this end, multiple approaches including rational engineering of surface epitopes on AAV capsids, directed evolution through DNA shuffling, peptide insert libraries, 3D structure-guided evolution, and more recently, machine learning, have been used to generate AAV variants with altered tropism, improved transduction efficiency and/or the ability to evade neutralizing antisera[16–20]. We have recently demonstrated the feasibility of achieving receptor switching in evolved AAV variants through infectious cycling of AAV capsid libraries with modified surface footprints[21].

In this study, we adapted a structure-guided evolution approach to evolve an AAV variant that we term Ark313, which is derived from AAV6 and exhibits high transduction efficiency in murine T cells. We find that Ark313 can be used for transient gene delivery and precise genome engineering. Ark313 can be used to model various engineering strategies from human T cells in the murine context, and we present gene targeting strategies that expand the use of genetically engineered T cells for *in vivo* studies. Furthermore, through a genome-wide knockout screen, we identify an essential murine host factor and the mechanism for Ark313 cellular entry. Ark313 opens avenues in experimental T cell immunology and the preclinical modeling of precision-engineered cell therapies in immunocompetent hosts.

RESULTS

Structure-guided evolution identifies an AAV capsid variant with murine T cell tropism

To identify an AAV variant enabling efficient DNA delivery to murine T cells, we generated an AAV capsid library based on AAV serotype 6. This serotype was chosen as a template for mutagenesis and evolution due to its established ability to transduce and facilitate HDRT knock-in in human T lymphocytes, NK cells, and hematopoietic stem cells[6,22,23]. We performed saturation mutagenesis on a pseudotyped AAV2/6 wild-type genome composed of the AAV2 Rep gene and AAV6 Cap gene flanked by AAV2 inverted terminal repeats (ITRs). Saturation mutagenesis was performed on variable region IV (VR-IV) (amino acids 454–460) of the VP3 capsid protein subunit. This surface epitope has been implicated in host cell entry and antibody-mediated neutralization of different AAV serotypes. We have

previously shown that targeting this region in other AAV serotypes for structure-guided evolution can yield improved variants[21,24].

We developed a screening strategy to identify AAVs that could efficiently deliver donor DNA to murine T cells for CRISPR/Cas9 genome editing. Primary splenocyte T cells isolated from C57BL/6J mice were activated with CD3/CD28 beads and recombinant IL-2 and then co-cultured with the capsid library at a low multiplicity of infection (MOI) of 1×10^4 (Fig. 1A). To enrich for mutants that had undergone cellular uptake, T cells were washed post-infection to remove residual surface-bound virus. The viral DNA that remained was purified, PCR-amplified, and re-cloned into the wild type AAV plasmid backbone to generate a capsid library for a subsequent round of evolution (Fig. 1A). After three infection cycles, the parental and evolved libraries were analyzed by next-generation sequencing. Remarkably, a single dominant variant that we termed Ark313, which carried the amino acid substitution 454-VVNPAEG-460, displayed ~200,000-fold enrichment from the parental library (Fig. 1B, Fig. S1A). Evaluation of the top-ranked sequences and most highly enriched reads (top 50 reads with more than 500-fold enrichment) indicated a consensus motif [I/V][I/L/V][N][P] for the first four amino acids (Fig. 1C, Fig. S1B,C).

We produced recombinant AAV6 and Ark313 and observed no significant difference for viral titer between AAV6 and Ark313, suggesting that the mutations did not affect packaging efficiency (Fig. 1D). We then assessed the AAVs for cell surface binding and uptake. Murine T cells were cooled to 4°C prior to and during AAV incubation to arrest cellular uptake. After washing cells to remove unbound virus, viral DNA was extracted, and the number of vector genomes per cell was quantitated. Compared to AAV6, a significantly higher amount of Ark313 was bound to murine T cells (Fig 1E). To analyze cellular uptake, the same process was performed to allow AAV binding, followed by a short incubation at 37°C to promote uptake. A significantly higher percentage of Ark313 particles compared to AAV6 was internalized by murine T cells (Fig 1F). After observing the enhanced binding and uptake of Ark313, we evaluated transduction. We packaged a self-complementary AAV (scAAV) encoding GFP under a hybrid chicken β-actin (CBh) promoter in either AAV6 or Ark313 capsids (Fig. 1G). In human T cells, high transduction efficiency was observed with AAV6 as expected at MOIs 10^4, and only minimal GFP expression observed with Ark313 at the highest MOI (Fig. 1H, Fig. S1D). These data suggest that the VR-IV of the AAV6 capsid is critical for AAV6 entry in human T cells. Remarkably, in murine T cells, Ark313 exhibited improved transduction efficiency compared to AAV6 by a 30-fold increase in mean fluorescence intensity (MFI) at a low MOI and up to 46-fold at higher MOIs (Fig. 1I, Fig. S1E). Improved transduction was observed using Ark313 compared to AAV6 with both scAAV and single-stranded AAV (Fig. S1F). Together, these results demonstrate that Ark313 has high transduction efficiency in murine T cells and suggest the involvement of a murine T cell-specific host factor in Ark313 binding and uptake.

Genome-wide CRISPR/Cas9 screen identifies essential genes for Ark313 transduction

The primary cellular entry mechanisms for AAV6 in human T cells have not been specifically explored, but the role of heparan sulfate and N-linked sialylated glycoproteins[25–27] and the cognate AAV receptor (AAVR)[28] in cell surface binding and

uptake in general are understood. To determine the entry mechanism of Ark313, we optimized a flow cytometry-based genome-wide CRISPR KO screen to identify host factors required for Ark313 transduction in primary murine T cells (Fig. 2A). Activated Cas9-expressing murine T cells were transduced with a γ-retroviral pool containing a genome-wide sgRNA library (90,230 sgRNAs)[29] and transduced with an Ark313 scAAV for GFP expression at an MOI of 3×10^4. Cells were sorted into four bins for low-to-high GFP expression (Fig. 2B). Genomic DNA was extracted from each sorted population, and sgRNA barcodes were PCR-amplified and sequenced. gRNAs enrichment in each of the four bins was compared using Waterbear analysis, and sgRNAs were ranked based on enrichment in lower GFP bins, revealing 15 genes as positive regulators of Ark313 transduction with a local false sign rate *(lfsr)* < 0.1 (Fig. 2C). The top hits included genes that are known to be involved in AAV transduction. As expected, *AU040320*, encoding the previously described AAVR[28], was highly enriched (Fig. 2C,D). Encouragingly, we also identified *Gpr108* (Fig. 2C,D), which has been identified together with AAVR as an important regulator of AAV processing[28,30]. Both hits provided confidence in the sensitivity of the screen. Among the remaining top hits identified were *B2m*, *H2-Q7*, and *H2-Q6*, which are components of major histocompatibility complex (MHC) class I (Fig. 2E). *H2-Q7* and *H2-Q6,* together with *H2-Q8* and *H2-Q9*, encode proteins that are classified as QA2[31]. Interestingly, H2-Q7 is a GPI-anchored cell surface protein[32–34], and multiple GPI-processing genes such as *Gpaa1* were also identified as top hits (Fig. 2D,E). In summary, the screen identified known regulators of AAV transduction and nominated the MHC class I molecule QA2 as a necessary host factor for Ark313 transduction.

To further validate the hits from the screen, we nucleofected activated T cells in arrayed format with RNPs containing two separate sgRNAs for knocking out each gene (Fig. S2A,B). Nucleofected cells were then reactivated and transduced with scAAV-GFP in Ark313. We observed nearly complete prevention of GFP expression, and thus transduction, in cells that had undergone knockout of *B2m*, *H2-Q7*, or *Aavr* (Fig. 2F, Fig. S2B). GFP expression was also reduced in *Gpr108*-KO cells (Fig. 2F, Fig. S2B), though to a lower extent than in other KO cells, consistent with the gene effect in the screen (Fig. 2D). Because H2-Q7 is a GPI-anchored protein (Fig. 2E), we assessed the ability of Ark313 to transduce murine T cells pre-treated with recombinant GPI-cleaving enzyme phosphoinositide phospholipase C (PI-PLC). We first tested binding of AAV6 or Ark313 to T cells with or without PI-PLC pre-treatment. AAV6 was not affected in its ability to bind C57BL/6J T cells, but Ark313 had a ~10-fold reduction in bound virus per cell (based on quantification of viral genomes) following PI-PLC treatment (Fig. 2G). We next assessed if GPI cleavage could ablate Ark313 transduction. Following PI-PLC pre-treatment, the Ark313 condition had a ~5-fold decrease in the percentage of GFP-positive cells, exhibiting similar transduction as the AAV6, whereas AAV6 remained unaffected (Fig. 2H). These data corroborate the finding that the GPI-anchored protein H2-Q7 is essential for Ark313 binding and transduction of murine T cells.

To validate the requirement of QA2 expression for Ark313 transduction, we isolated and activated T cells from mouse strains that express various levels of QA2. In addition to C57BL/6J, BALB/cJ was included as a control strain that expresses low QA2 as a result of Q8/Q9 genetic deletions[34–36], as well as NOD mice, which express an intermediate

level of QA2 (Fig. S2C). T cells were transduced with scAAV-GFP packaged in either AAV6 or Ark313 and analyzed by flow cytometry. Within each strain, GFP expression was higher in QA2-high cells, especially for C57BL/6J and NOD (Fig. S2D). In contrast, AAV6 transduction efficiency was low and equivalent regardless of QA2 expression (Fig. S2C,D). To further validate the role of QA2 in Ark313 infection we transduced $QA2^{null}$ T cells isolated from BALB/cByJ mice with a gRV encoding H2-Q7 (Fig. 2I). The cells were subsequently transduced with scAAV-GFP in Ark313 and analyzed by flow cytometry. GFP expression was significantly higher in H2-Q7-overexpressing cells (Fig. 2J). These results suggest that QA2 is an essential host factor for Ark313 transduction.

Given Ark313 uses an MHC class I molecule as a required host factor, we next assessed if Ark313 transduction impacts MHC class I expression and T cell engraftment *in vivo*. We transduced CD45.1 T cells with either a scAAV-GFP in Ark313 or a gRV expressing GFP and injected the cells retro-orbitally in C57BL/6J mice (Fig. S2E). Spleens were harvested after 7 and 14 days, and no differences in engraftment was observed (Fig. S2F). Interestingly, although the Ark313-transduced T cells expressed the same levels of B2M and QA2 compared to host T cells (Fig. S2G,H), the gRV-transduced cells had increased levels of B2M (Fig. S2G,H).

Ark313 enables efficient gene targeting in primary murine T cells

We hypothesized that the superior transduction of primary murine T cells by Ark313 could be applied to gene editing. We first tested if Ark313 could deliver an sgRNA expression cassette. T cells were isolated from Cas9-expressing mice, activated, and transduced with Ark313 expressing either a *Trac*-targeting sgRNA or a scrambled (SCR) control sgRNA (Fig. 3A). Analysis of TCR expression by flow cytometry indicated up to 84% knockout in the *Trac*-sgRNA-transduced cells (Fig. 3B, Fig. S3A). Even at the lowest MOI tested, the KO efficiency was above 40% (Fig. S3A). To determine the frequency of non-specific Ark313 integration in the presence of a double-strand break (DSB)[37], Cas9-expressing T cells were transduced with a scAAV-GFP with or without a *Trac*-sgRNA. GFP expression in scAAV-GFP-treated cells was transient, whereas there was a rare population (<0.6%) of cells that maintained high GFP expression (consistent with integration) in the presence of a DSB (Fig. S3B,C). Although non-specific AAV integration in the presence of a DSB is a concern when using AAVs for gene editing, our results show that non-specific integration of Ark313 is a rare event.

Next, we assessed if Ark313 could deliver larger DNA cargo such as an HDRT for knock-in and target a GFP to the broadly expressed clathrin light chain A (*Clta*) locus. Murine T cells were nucleofected with Cas9-RNP targeting the *Clta* gene, and cells were transduced with either AAV6 or Ark313 containing an HDRT for fusing GFP to the *Clta* N-terminus (Fig. 3C). AAV6 was inefficient at delivering HDRT, with less than 10% knock-in at the highest MOI. Remarkably, Ark313 yielded much higher knock-in: above 30% at the lowest MOI tested and beyond 50% at the highest MOI (Fig. 3D). The targeted integrations were further validated by PCR amplification of genomic DNA flanking the targeted locus (Fig. S3D).

Although knock-in efficiency was greatly improved with Ark313, we sought to reduce the cell loss associated with RNP nucleofection (Fig. S3E-G) and further improve the edited

cell yield. Since Ark313 provided high gene editing efficiency in delivering an sgRNA (Fig. 3B, Fig. S3A), we hypothesized that co-delivery of sgRNA and HDRT in a single vector to T cells that constitutively express Cas9 would result in efficient knock-in and low toxicity. We incorporated a U6 promoter expressing a *Clta*-targeting sgRNA adjacent to the HDRT for the GFP-*Clta* fusion and packaged this vector into either Ark313 or AAV6 (Fig. 3E). Cas9-expressing T cells transduced with AAV6 had no detectable knock-in across a range of MOIs. Strikingly, Ark313-mediated co-delivery of sgRNA and HDRT resulted in a knock-in efficiency similar to that observed with Cas9-RNP nucleofection (Fig. 3F). There was no substantial difference in proliferation or cell numbers between non-treated cells and Ark313-treated cells (Fig. 3G), and the nucleofection-free method increased the knock-in cell yield by over five-fold (Fig. 3H). These data underscore the superior performance of Ark313 for both transient gene delivery and targeted integration in primary murine T cells. The high transduction efficiency of Ark313, which allows for co-delivery of an HDRT and sgRNA, enables one-step manufacturing of knock-in cells with high viability and should facilitate large-scale production of T cells for *in vitro* and *in vivo* applications.

Targeting recombinant receptors to the *Trac* locus for experimental T cell immunology

Because Ark313-mediated gene delivery unlocked the capability to perform knock-ins in T cells, we sought to expand the use of Ark313 to engineer T cells for the study of adoptive cell therapies against cancers. We designed an HDRT targeting *Trac* exon 1 for expression of a transgene under the endogenous promoter and integrated receptors that are relevant to immunotherapy such as a murine CAR targeting human CD19 (hCD19) (h19m28z), a HIT targeting hCD19, or a transgenic OT-I TCR (Fig. 4A). We also generated a construct for rescuing *Trac* expression to generate TCR-positive *Trac*-CAR-T cells (Fig. 4A). Each vector contained a U6 promotor-driven *Trac* sgRNA for nucleofection-free editing and was packaged in Ark313.

We first transduced activated T cells from Cas9-expressing mice with a *Trac*-CAR in Ark313 at several MOIs. Flow cytometry analysis indicated efficient CAR knock-in (up to 45% at the highest MOI) and homogenous CAR expression (Fig. 4B, Fig. S4A,B). When combined with an NHEJ inhibitor (M3814), Ark313 mediated KI reached up to 75% (Fig. S4C). A comparison of edited cell yield using Cas9-RNP nucleofection vs. nucleofection-free knock-in by co-delivery of sgRNA and HDRT indicated a ~10-fold increase in *Trac*-CAR cells using the nucleofection-free approach (Fig. S4D,E). To validate the functionality of the antigen-specific *Trac*-T cells (Fig 4C), we performed a cytotoxicity assay with hCD19-expressing murine Lewis lung carcinoma cancer cells (LL2-hCD19) (Fig. S4F). Compared to non-transduced T cells, each of the hCD19-targeting T cell conditions exhibited significant cytotoxicity against antigen-expressing cells (Fig. 4D). We also validated the functionality of the *Trac*-OT-I TCR-T cells through an assay with OVA-expressing B78 cells and observed that *Trac*-OT-I TCR knock-in cells exhibited similar cytotoxicity as did transgenic (Trg) OT-I TCR-T cells (Fig. 4E). Lastly, as the field of synthetic immunology is moving towards larger cassettes and multiplex edits, we sought to demonstrate the potential of Ark313 in facilitating either large transgene insertion (Fig. S4G) or multiple genetic modifications in a single step. Cas9-expressing T cells were transduced with two separate Ark313 all-in-one HDRTs targeting two separate genes, *Clta*

and *Trac*. Over 8% of cells underwent dual knock-in (Fig. 4F), further highlighting the range of use for Ark313 in engineering complex gene-edited T cell therapies.

Targeting a CAR to the *Trac* locus with Ark313 enhances tumor control in an immunocompetent solid tumor mouse model

We have previously demonstrated that human *TRAC*-CAR-T cells are superior to retrovirally engineered CAR-T cells in controlling a B-ALL xenografted tumor. To explore whether the superiority of *TRAC*-CAR-T cells is maintained in an immunocompetent solid tumor model, we extended previously tested receptors[7] to the murine context. We generated *Trac*-CAR-T cells with Ark313 and conventional CAR-T cells with gRV, both expressing the same h19m28z. To facilitate more comparisons with *Trac*-CAR-T cells, which are TCR-KO, the gRV-expressing CAR-T cells were co-transduced with Ark313 expressing either a *Trac*-targeting sgRNA or SCR sgRNA (Fig. 5A), generating TCR-KO gRV-CAR-T cells or TCR-intact gRV-CAR-T cells, respectively. CAR and TCR expression were assessed by flow cytometry prior to T cell injections (Fig. 5B). LL2-hCD19 cells were injected subcutaneously in C57BL/6J mice, and nine days later, a single dose of either *Trac*-CAR-T cells or gRV-CAR-T cells was injected retro-orbitally (Fig. 5A). Interestingly, although the gRV-CAR-T cells were highly cytotoxic *in vitro* (Fig. S5A), their control of the tumor *in vivo* was limited (Fig. 5C), with no significant improvement in survival compared to non-treated mice at this dose (Fig. 5D). However, the *Trac*-CAR-T cells reduced tumor size and significantly improved survival compared to non-treated mice in this highly aggressive solid tumor model (Fig. 5C,D).

To further characterize CAR-T cells in vivo, in a separate experiment, we harvested LL2-hCD19 tumors and draining lymph nodes (dLN) eight days after injection with *Trac*-CAR-T cells or TCR-KO gRV-CAR-T cells (Fig. 5E). We used CAR constructs that co-expressed Thy1.1 to quantify CAR-T cell infiltration (Fig. S5B). The average tumor weight was significantly lower in the *Trac*-CAR-T cell group (Fig 5F), confirming the improved anti-tumor activity of the *Trac*-CAR-T cells as compared to gRV-CAR-T cells. The total number of CAR-T cells per tumor was similar (Fig. 5F), however there were significant increases in the CAR-T cells per mg tumor tissue and the total CAR-T cells in dLNs (Fig. 5F).

We previously demonstrated in human T cells that the endogenous *TRAC* locus confers optimal CAR replenishment after antigen-induced CAR downregulation from the cell surface and delayed effector T cell differentiation[7]. To define the role of the murine *Trac* locus in controlling CAR expression, we performed a repetitive stimulation assay and measured CAR surface expression over time. As in human T cells, CAR expression decreased in both *Trac*-CAR-T and gRV-CAR-T cells after antigen engagement, with a slower return to baseline in the *Trac*-CAR-T cells (Fig. 5G, Fig. S5C). A similar pattern was observed with two stimulations where the gRV-CAR-T cells recovered CAR expression faster than *Trac*-CAR-T cells (Fig. 5G). Finally, *Trac*-CAR-T cells displayed an increase in the central memory phenotype upon one and two stimulations as compared to gRV-CAR-T cells (Fig. 5H).

The findings recapitulate the improved efficacy of the human *TRAC*-CAR counterpart[7] and highlight the utility of Ark313 in testing next-generation T cell therapies in immunocompetent settings.

DISCUSSION

We applied structure-guided evolution to discover an AAV that has tropism for murine T lymphocytes. This discovery approach could in principle be extended to any AAV capsid to target other cell types of interest. We focused on murine T cells to enable targeted manipulation in immunocompetent mouse models. Many clinical trials use adoptive T cell therapies, and more recently precisely edited T cells (NCT03666000, NCT04035434, NCT04629729, NCT04637763). However, to date, murine T cell engineering has relied on the use of transgenic mice or semi-randomly integrating viral vectors, as gene targeting has been inefficient and HDRT DNA delivery can be toxic. While AAV5 has been used for gene targeting in murine T cells[38], it still lacks the efficiency seen in human T cells. The inability to perform gene targeting at high efficiencies in mouse models has been a roadblock for T cell immunology and preclinical modeling in immunocompetent mice. Therefore, Ark313 is a potentially transformative tool for T cell immunology and cancer immunotherapy.

Genome-wide screens have been used to identify essential host factors and restriction factors for viruses. In the case of AAV, a genome-wide perturbation screen for infection host factors was performed with AAV2 on the HAP1 human cell line, which identified *AAVR* and *GPR108*[28]. Subsequent efforts by our group identified host restriction factors such as *Crb3*[39] and also receptor switching mechanisms in evolved AAV variants[21]. We identified that the VR-IV region in AAV8 can be evolved to a variant, Hum.8, which uses integrin beta-1 (ITGB1) in lieu of the cognate AAVR, demonstrating the evolutionary plasticity in AAV tropism. In the current study, we identified essential cell surface binders of Ark313, through a genome-wide knockout screen on primary T cells. The screen highlighted known essential genes for AAV processing, *Aavr* and *Gpr108*[28], and *B2m* and *H2-Q7* were among the top hits (Fig. 2C,D,F). B2M is a protein that associates with MHC class I, and H2-Q7 is a protein that along with Q5, Q6, Q9, and Q10 is referred to as QA2. The connection between Ark313 and MHC class I led us to hypothesize that the human ortholog for H2-Q7, HLA-G[33,40], might mediate AAV6 uptake in human T cells, but *B2M* KO in human T cells or HLA-G expression did not affect AAV6 transduction (Fig. S5F,G). Looking forward, we anticipate that the screen design here could be extended to identify primary receptors for other AAV serotypes.

We observed that Ark313 transduction correlated with QA2 expression using cells from different mouse strains (Fig. S2C). With this correlation, gene expression databases can be used to hypothesize which cell types might be amenable to Ark313 transduction. For example, NK and NKT cells express *H2-Q7*/QA2[41] and therefore might be good candidates, which would provide possibilities to study engineered NK cells in immunocompetent mice. Conversely, neutrophils, monocytes, macrophages, and certain B cell subsets express low levels of *H2-Q7*/QA2[41,42], so we predict low transduction efficiency. Both our AAV library approach and KO screen could be extended to these cell types to generate AAV variants and interrogate the biology of virus-host interactions.

We showed that Ark313 is an efficient vector for transient transgene expression in murine T cells by expressing GFP or an sgRNA. This approach requires minimal cell handling, is non-toxic and easily scalable, and can be applied to any transgene within packaging capacity such as Cre, compact Cas proteins[43], or genes that might modulate T cell function or fate. Ark313 also permits non-toxic HDRT delivery for efficient gene targeting. We observed >50% knock-in at the *Clta* locus by delivering the HDRT with Ark313 to RNP-nucleofected cells (Fig. 3D). There was on average a ~60% reduction in cell viability and slower proliferation in the days after murine T cell nucleofection, which is substantially worse than the analogous viability reduction for human T cells. This cell loss potentially limits the use of edited mouse T cells in large-scale experiments, such as those with libraries. We overcame this technical hurdle by successfully co-delivering HDRT and sgRNA in a single AAV to Cas9-expressing cells (Fig. 3E). Nucleofection-free knock-in yielded similar efficiencies as with nucleofection but without the negative impact on cell yield (Fig. 3F,G). Although the packaging capacity of AAV vectors imposes limits on cargo delivery, we showed that dual knock-in can be achieved by co-transduction of multiple AAVs, which should facilitate a variety of engineering and screening applications (Fig. 4F).

Using the mouse *Trac* locus, we can now integrate receptors and explore their functionality and limitations in immunocompetent model systems. We targeted a CAR, HIT, and transgenic TCR to the *Trac* locus using the Ark313 nucleofection-free approach (Fig. 4A,C). These three families of receptors, when delivered to the human *TRAC* locus, are in clinical or in pre-clinical stages of development but have yet to be tested in complex immunocompetent models that recapitulate the challenges that T cell therapies encounter in solid tumors. Human *TRAC*-CAR-T cells have been demonstrated to improve tumor clearance in xenograft models compared to conventional virally expressed CAR-T cells[7]. We compared murine *Trac*-CAR-T cells and gRV CAR-T cells in an immunocompetent solid tumor mouse model, and only the *Trac*-CAR-T cells showed significant improvement in survival (Fig. 5D). The murine *Trac* locus also recapitulates the homogenous and predictable CAR expression as well as the optimal recovery of baseline CAR expression following antigen stimulation. This model should enable in-depth interrogation of the biology of *Trac*-CAR-T cells and how the cells interact with the endogenous immune system upon adoptive transfer.

Crosstalk between CARs and TCRs in solid tumors is currently not well understood. The TCR is known to contribute to T cell fitness through tonic signaling[44] and interaction with specific intra-tumoral DC populations, providing co-stimulation[45]. TCRs can also drive polyclonal antitumor responses that aid T cells in combating tumor heterogeneity. For *TRAC*-CAR T cells, the absence of a TCR might be beneficial, as co-activation of T cells through the CAR and the TCR has been shown to negatively affect CD8+ T cells in a leukemia model[46]. Our ability to generate a panel of TCR-expressing *Trac*-CAR-T cells by either knocking out of the TCR, rescuing the *Trac* gene, or co-delivering a recombinant TCR provides a path to study the interplay between CAR and TCR signaling *in vivo*. These results further highlight the potential impact of Ark313 as a tool in the field of T cell immunology.

The homogenous and monoallelic expression conferred by the *TRAC* locus has been demonstrated to be ideal for screening pooled libraries of genes in human T cells[47]. However, the relevance of the discovered genetic effects depends on the biological context. In this study, we show similar homogenous and predictable expression at the *Trac* locus of murine T cells (Fig. S5F), and therefore Ark313 offers the possibility pooled library screening at *Trac* in immunocompetent models. Finally, while our study focuses on cancer immunotherapy, applications for redirecting T cell specificity extend beyond cancer mouse models. The potential to knock in any TCR to replace the endogenous TCR, without the need to breed transgenic TCR mice, opens possibilities to study T cells in autoimmunity. We expect that Ark313 will be a fundamental tool to accelerate the discovery of cell therapy modalities in immunocompetent models and clinical translation.

Limitations of the study

We observed that both AAV transduction efficiency and gene targeting efficiency is greatly improved in activated T cells compared to naïve T cells. This potentially limits the use of Ark313 for certain applications needing naïve T cells. A further limitation is that Ark313 requires QA2 surface expression for efficient transduction, QA2 expression varies across mouse strains and potentially limits the use of Ark313 for certain mouse strains, such as BALB/c mice. Furthermore, we showed that overexpression of QA2 in a QA2^{null} mouse strain improved Ark313 transduction, however, overexpressing QA2 was challenging and did not result in large increases of QA2 expression. Different strategies for overexpression need to be explored for robust QA2 overexpression.

STAR METHODS

RESOURCE AVAILABITY

Lead contact—Further information and requests for resources and reagents should be directed to and will be fulfilled by the lead contact, Justin Eyquem (justin.eyquem@ucsf.edu).

Materials availability

- Plasmids generated in this are available upon request.

- Restriction apply to the Ark313 plasmid availability due a material transfer agreement.

Data and code availability

- Sequencing data has been deposited at GEO and is publicly available and listed in the key resource table.

- Original code has been deposited at Zenodo and is publicly available and listed in the key resource table.

EXPERIMENTAL MODEL AND SUBJECT DETAILS

Mouse strains—Mice between 6–16 weeks of age were used following a protocol approved by the UCSF Institutional Animal Care and Use Committee and were housed

with a 12 h/12 h light/dark cycle and food/water available *ad libitum*. The following mouse strains were obtained from The Jackson Laboratory: C57BL/6J (#000664), BALB/cJ (#000651), BALB/cByJ (#001026), H11-Cas9 on C57BL/6J (#028239), *Rosa26*-Cas9 knock-in on C57BL/6J (#026179), and C57BL/6J-Ptprcem6Lutzy/J (#033076). NOD mice were bred and provided by the Qizhi Tang laboratory (UCSF). Female mice were used for all in vivo experiments.

Cell lines—All cell lines were maintained in sterile conditions in a 5% CO_2 incubator at 37°C.

Retroviruses and AAVs were each packaged in HEK293T cells (ATCC #CRL-3216). LL2-Luc2 cells (ATCC #CRL-1642-LUC2) were transduced with an MSCV retrovirus for expressing hCD19 and a puromycin resistance gene, and cells were selected with puromycin (2 μg/ml) for three days. Puromycin was subsequently maintained in the culture medium for these cells. OVA-expressing mCherry-positive B78 cells were provided by the Matthew Krummel laboratory (UCSF) and were used for assays with OT-I TCR T cells. These cell lines were cultured in GlutaMAX DMEM (Gibco #10566024) supplemented with FBS (10%; Corning #35016CV), penicillin-streptomycin (100 U/ml; ThermoFisher Scientific #15140122), sodium pyruvate (1 mM; Gibco #11360070), and HEPES (10 mM; Corning #25–060-CI).

The 721.221 HLA-negative B cell line (Millipore Sigma #SCC275) was cultured in RPMI 1640 (Gibco #11875093) supplemented with FBS (10%), penicillin-streptomycin (100 U/ml), sodium pyruvate (1 mM), HEPES (10 mM), β-mercaptoethanol (Gibco #21985–023), and MEM non-essential amino acids (1×; Gibco #11140050). The HLA-G-expressing 721.221 cell line was kindly provided by the Lewis Lanier laboratory (UCSF) and cultured under the same conditions as its parental cell line.

Primary cells—Murine T cells were cultured in RPMI 1640 (Gibco #11875093) supplemented with FBS (10%), penicillin-streptomycin (100 U/ml), sodium pyruvate (1 mM), HEPES (10 mM), β-mercaptoethanol (Gibco #21985–023), MEM non-essential amino acids (1×; Gibco #11140050) and hIL-2 (200 U/ml: Peprotech #200–02).

Human T cells were cultured in X-VIVO 15 medium (Lonza #BP04–744Q) supplemented with human serum (5%:Gemini Bioproducts #100–512), IL-7 (5 ng/ml: Miltenyi Biotec #130–095-367), and IL-15 (5 ng/ml: Miltenyi Biotec #130–095-760) at a density of 1×10^6 cells per ml.

METHOD DETAILS

Plasmids—Two scAAV vectors were produced for transiently expressing GFP, either scAAV-CBh-GFP[48] or a CMV enhancer chicken β-actin intron (CAG) promoter (scAAV-CAG-GFP, Addgene #83279). The two vectors are distinguished in the text and figure legends. For gRV expressed GFP, MSCV-Puro-EFS:GFP (Addgene #68484) was used).

To generate a GFP fusion at the *Clta* N-terminus, the GFP gene was cloned into an AAV plasmid containing homology arms targeting the *Clta* exon 1 start codon. LHA (351

bp) and RHA (303 bp) sequences are listed the primers and sequences section below. For nucleofection-free knock-in, a U6 promoter for expressing a *Clta*-targeting sgRNA (AUGGCCGAGUUGGAUCCAUU) was introduced upstream of the LHA.

For integrating genes at the *Trac* locus, homology arms targeting *Trac* exon 1 were cloned into an AAV plasmid. LHA (497 bp) and RHA (500 bp) sequences are listed in the primers and sequences section below. Genes for either 1928z CAR (flanked by P2A sequences), hCD19-targeting HIT, or OT-I TCR were cloned between the homology arms, a P2A sequence and the Thy1.1 gene were included downstream of the CAR. To generate a TCR rescue construct, a gene fragment to rescue *Trac* was introduced upstream of the 1928z P2A. For nucleofection-free knock-in, a U6 promoter for expressing a *Trac*-targeting sgRNA (UAUGGAUUCCAAGAGCAAUG) was introduced upstream of the LHA.

For retroviral expression under the 5' LTR promoter, the 1928z CAR was cloned into an MSCV plasmid, and a P2A sequence and the Thy1.1 gene were included downstream of the CAR.

Knockouts with Ark313 used a U6 promotor to express either a scrambled (SCR) negative control sgRNA (GGCAGGUCGCCGCGCGUAAU) or a *Trac*-targeting sgRNA (UAUGGAUUCCAAGAGCAAUG). For H2-Q7 overexpression, the cDNA sequence was cloned in with a P2A-mKate sequence in place of GFP in the MSCV-Puro-EFS:GFP plasmid. A control plasmid with mKate only was cloned for control purposes.

AAV production—AAV2-ITR containing plasmids were utilized to package vector genomes into different AAV capsids by transfection of HEK293T cells together with adenovirus helper and AAV Rep-Cap plasmids using polyethylenimine (Polysciences #23966). 293T cells were seeded in 150 mm plates, each plate was transfected with 6 μg cargo vector, 8 μg of Rep-Cap plasmid, 11 μg of adenovirus helper plasmid in 200 μl PEI for 72 hours. Transfected 293T cells were collected in AAV lysis buffer (50 mM Tris, 150 mM NaCl) and lysed by three rounds of rapid freeze/thawing, followed by a 1 h incubation at 37°C with 25 units/ml Benzonase (Millipore Sigma #70–664-3). AAV vectors were further purified following cell harvest and PEG precipitation using iodixanol (OptiPrep, StemCell Technologies #07820) gradient ultracentrifugation. AAV vector titers were determined by qPCR on DNaseI (NEB #B0303S) treated, Proteinase K (Qiagen #1114886) digested AAV samples post-purification, using primers targeting the viral genome. qPCR was performed with SsoFast Eva Green Supermix (Bio-Rad #1725201) on a StepOnePlus Real-Time PCR System (Applied Biosystems #4376600). Relative quantity was estimated by comparison to a serial dilution of a vector plasmid standard of known concentration.

AAV transduction—Unless otherwise specified, AAV transduction of T cells was performed as follows. T cells activated by Dynabeads (24 h for murine cells and 48 h for human cells) were seeded at 2×10^6 cells per ml in T cell medium, and AAV was added at a specified MOI. It was ensured that the volume of AAV added did not exceeded 20% of the culture volume. After incubating the culture overnight, the AAV-containing medium was exchanged for fresh medium, and the T cells were subsequently cultured in standard conditions.

Generating and Cycling of the AAV6 capsid library—The AAV6 capsid library was generated by performing saturation mutagenesis of seven residues in the VR-IV region as reported previously[24]. Briefly, to generate the library, an overlap extension PCR was performed using two amplicons amplified from a modified AAV6 backbone containing seven tandem stop codons replacing the randomized region (amino acids 454–460 VP1 numbering) to prevent potential amplification of the wild type sequence. The first amplicon consisted of 34 bp of the AAV6 cap immediately 5' of the randomized region, the randomized region, and the AAV6 Cap up to the Sbf1 site 3' of the randomized region. The second amplicon consisted of the AAV6 cap starting from the BsiWi site 5' of the randomized region up to the 34 bp of the AAV6 cap immediately 5' of the randomized region. The two resulting amplicons were combined in equimolar ratio in a second PCR for overlap extension. The final assembled amplicon was digested using BsiWI-HF (NEB #R3553S) and SbfI-HF (NEB #R3642S)and ligated into the pITR2-Rep2-dead(GFP)Cap6 backbone using T4 DNA ligase (NEB #M0202S). The pITR2-Rep2-dead(GFP)Cap6contains AAV2 ITRs and Rep along with the AAV6 Cap gene interrupted by a filler sequence derived from GFP inserted out of frame into the cognate BsiWI and SbfI site to eliminate any potential wild type AAV6 from the library ligation. Ligation products were concentrated and purified by ethanol precipitation. Purified products were electroporated into DH10B ElectroMax cells (Invitrogen #18290015) and directly plated on multiple 5,245-mm^2 bioassay dishes (Corning #431111) with LB/ampicillin agar to maintain library diversity. Plasmid DNA from AAV6 capsid libraries was purified from pooled colonies grown on LB agar plates with ampicillin using a ZymoPURE II plasmid maxiprep kit (Zymo Research #D4203.

AAV6 capsid libraries were produced by cotransfection of adherent HEK293 cells with adenovirus helper plasmid (pXX680[49], 19.25 μg/plate) and the Rep Cap plasmid library (8.75 μg/plate) mixed in a 3:1 ratio with PEI MAX (Polysciences #24765–1). Viral media was collected at day 4 and 6, and the cell pellet at day 6. Media was PEG precipitated and the cell pellet was triton lysed before pooling and purification by iodixanol density gradient ultracentrifugation. To evolve the library activated murine T cells were seeded at 1×10^6 cells per ml and transduced with the pooled AAV6 capsid library for 6 h at an MOI of 1×10^4vg/cell. Then, the cells were washed twice with PBS to remove any unbound AAV, and cellular and viral DNA was extracted from cells using an IBI genomic DNA extraction kit (IBI Scientific #IB47280). The Cap region was amplified by PCR before being digested and ligated back into the pITR2-Rep2-dead(GFP)Cap6 backbone to generate the next-round library. The process of library production, AAV packaging, T cell transduction, and viral DNA extraction was performed three times to generate the evolved library.

AAV6 capsid library sequencing and analysis—Parental and evolved libraries were processed for Illumina NovaSeq sequencing. Parental and evolved libraries were each treated with DNase I and purified by iodixanol gradient centrifugation. To dissociate the capsid, virus was heated in a PCR tube (95°C, 15 min) with Tween-20, which prohibits capsid reassembly that would interfere with amplification. Round 1 PCR was performed with primer sets F:5'-CCCTACACGACGCTCTTCCGATCT**NNNNN**CTGGACCGGCTGATGAATCCTCTC-3'

and R:5'-
GACTGGAGTTCAGACGTGTGCTCTTCCGATCT**NNNNN**TATACGTCTCTGTCTTGCC
ACACCATTCC-3' for 18 cycles using Q5 polymerase (NEB #M0492S), and amplicons
were PCR-purified (IBI Scientific #IB47010). In round 2, indices for demultiplexing and the
P5 and P7 flow cell adaptor sequences were added in a 15-cycle PCR, and amplicons were
run on and purified from a 1% agarose gel. The amplicon band was gel-purified, amplicon
quality was verified using a Bioanalyzer (Agilent), and concentrations were quantified by
Qubit (Invitrogen). Libraries were prepared using the Illumina NovaSeq 6000 S-Prime
reagent kit (300 cycles, Illumina #20028312) following the manufacturer-provided
instructions and sequenced by Illumina NovaSeq.

De-multiplexed reads were analyzed using an in-house Perl script as done in another context
previously[21]. Reads were probed for the nucleotide sequences corresponding to the library
region, and the occurrence of each nucleotide sequence was counted and ranked. These
sequences were converted to amino acid sequences and pooled by like-sequence, counted,
and ordered by percentage rank. A second Perl script was used to calculate enrichment
between the evolved library and parental library as done previously[21]. Sequences were
plotted in Tableau with y-axis as log percentage, x-axis as a random dimensionless number,
and bubble size correlating to enrichment, where enrichment is the percentage of reads
of a variant from the evolved library divided by the percentage of reads of that variant
from the parental library. The frequency of each randomized amino acid in the library was
calculated, and heatmaps were generated in GraphPad Prism. To generate the amino acid
position-specific scoring matrix, sequences that were in the top 50 reads of the evolved
library and enriched by over 500-fold from the parental library were selected and run
through PSSMSearch (http://slim.icr.ac.uk/pssmsearch/).

Animal work—C57BL/6J mice between 6–8 weeks of age were injected subcutaneously
with 5×10^5 hCD19-expressing LL2/Luc2 cells. Nine days after the tumor cell injection,
mice were injected retro-orbitally with $1.5–2\times10^6$ CAR-T cells. The mice were pre-treated
with cyclophosphamide (100 mg/kg; Sigma Aldrich #C07681G) two days before the T cell
injections. Mice with small ($<20mm^3$) or ulcerated tumors at the day of T cell injections
were excluded from the experiment, the experimental groups were randomly allocated
among the remaining mice. Tumors were measured using a caliper, and tumor size was
estimated using the formula $V=(L\times W\times W)/2$. For tissue harvest, tumors were harvested
and processed in PBS using a GentleMACS Octo Dissociator (Miltenyi Biotec #130–
096-427) in gentleMACS C Tubes (Miltenyi Biotec #130–093-237). Dissociated tumors
were then digested in RPMI supplemented with 4 mg/ml Collagenase IV (Worthington
#LS004189) and 0.1 mg/ml DNase I (Millipore Sigma #10104159001) for 30 min at 37°C.
dLNs (inguinal, axillary and brachial) were isolated after and digested in RPMI (Gibco
#11875093) supplemented with 4 mg/ml Collagenase IV (Worthington #LS004189) and
0.1 mg/ml DNase I (Millipore Sigma #10104159001) for 30 min at 37°C. After tissue
digestions cells were washed in FACS buffer (2% FBS (Corning #35016CV) and 1 mM
EDTA (Invitrogen #15575020) in PBS) and strained using 70 μM Cell Strainers (Corning
#431751). Cells were then resuspended in FACS buffer and stained for flow cytometry.
Spleens were harvested, crushed in FACS buffer, strained and then treated with 1 ml ACK

lysing buffer (Quality biological #118–156-101) for 2 min. The lysing process was quenched by adding 20 ml FACS buffer, the cells were then strained and resuspended in FACS buffer and stained for flow cytometry.

T cell isolation and culture—Spleens from mice were crushed and strained, and T cells were isolated using an EasySep mouse T cell isolation kit (STEMCELL Technologies #19851) and activated for at least 24 h using Dynabeads Mouse T-Expander CD3/CD28 (Gibco #11452D). Murine T cells were cultured in RPMI 1640 (Gibco #11875093) supplemented with FBS (10%), penicillin-streptomycin (100 U/ml), sodium pyruvate (1 mM), HEPES (10 mM), β-mercaptoethanol (Gibco #21985–023), MEM non-essential amino acids (1×; Gibco #11140050) and hIL-2 (200 U/ml: Peprotech #200–02).

Human T cells were isolated from leukopaks with obtained from STEMCELL Technologies (# 70500.1). T lymphocytes were then purified using the EasySep Human T cell isolation kit (STEMCELL Technologies #17951) and activated with Dynabeads Human T-Activator CD3/CD28 (ThermoFisher #11131D) in X-VIVO 15 medium (Lonza #BP04–744Q) supplemented with human serum (5%:Gemini Bioproducts #100–512), IL-7 (5 ng/ml: Miltenyi Biotec #130–095-367), and IL-15 (5 ng/ml: Miltenyi Biotec #130–095-760) at a density of 1×10^6 cells per ml.

Flow cytometry—Cells were stained in 100 μl FACS buffer (2% FBS and 1 mM EDTA in PBS) for 30 min at room temperature using the following reagents at a 1:100 dilution: 7-AAD (eBioscience #00–6993-50), propidium iodide (MilliporeSigma #P4170), PE-Vio770 anti-mouse QA2 (Miltenyi Biotec #130–103-909), Vioblue anti-mouse QA2 (Miltenyi Biotec #130–103-905), APC-Cy7 anti-mouse TCRβ (BD #560656), Alexa Fluor 647 anti-mouse F(ab')$_2$ for the CAR (Jackson ImmunoResearch #115–606-003), BV421 anti-mouse TCRVα2 (BioLegend #127825), APC anti-mouse TCRβ5.1 (BioLegend #139506), BV421 anti-mouse CD90.1 (BioLegend #202529), BUV737 anti-human CD19 (BD biosciences #564303), BUV496 anti-human CD19 (BD biosciences #612938), BV711 anti-mouse CD8a (BD biosciences #563046), BUV395 anti-mouse CD4 (BD biosciences #740208), BUV737 anti-mouse CD90.2 (BD biosciences #741702), Alexa Fluor 647 anti-mouse CD90.2 (Biolegend #105318), BV605 anti-mouse CD62L (BD biosciences #563252), BUV737 anti-mouse CD44 (BD biosciences #612799), BUV605 anti-mouse B2M (BD biosciences #745120), BV421 anti-mouse CD45.1 (Biolegend #110731), BUV395 anti-mouse CD45.2 (BD biosciences #564616). Cells were stained in PBS during steps in which Zombie Violet (BioLegend #423114) or Ghost Dye Red 780 (Tonbo #13–0865-T100) were used at a dilution of 1:1000. Digested spleens, dLNs and tumors were first blocked using 10 μl of FcR Blocking Reagent Mouse (Miltenyi Biotec #130–092-575) in 100 μl FACS buffer at room temperature for 30 min before further antibody staining was performed.

For CAR detection, T cells were stained with Alexa Fluor 647 anti-mouse F(ab')$_2$ (Jackson ImmunoResearch #115–606-003) and then blocked with normal mouse serum (MilliporeSigma #NS03L) before further antibody staining was performed.

For quantification of cells during flow cytometry, 50 μl of CountBright Absolute Counting Beads (Invitrogen #C36950) were added to each sample following the manufacturers protocol.

Cytotoxicity assays—To evaluate the cytotoxicity of T cells expressing hCD19-targeting receptors, 1×10^4 hCD19-LL2-Luc2 cells were plated in 100 μl culture medium in a 96-well plate. 24 h later, 1×10^4 effector T cells in 50 μl culture medium were added to the wells. After 24 h of co-culture, luminescence was measured with a GloMax Explorer microplate reader (Promega #GM3500) by adding D-Luciferin (Goldbio #LUCK-1G) at a final concentration of 0.375 mg/ml to each well. The cytotoxicity for each sample was determined by the formula: 100%×(1–(sample–minimum)/(maximum–minimum)). The minimum signal was a condition with tumor cells and Tween-20 (0.2% v/v), and the maximum signal was a condition with tumor cells only.

To evaluate the cytotoxicity of OT-I TCR T cells, 1×10^4 OVA.mCherry.B78 cells were plated in 100 μl culture media in a 96-well plate. 24 h later, 2.5×10^3 effector T cells in 50 μl culture medium were added to the wells. Cells were co-cultured for five days with imaging at 2-h intervals using an Incucyte live-cell analysis instrument (Sartorius). The mCherry signal intensity from each well and time point was normalized to the average of the first time point in the control wells containing tumor cells only.

Assays for viral binding and cellular uptake—Murine T cells were activated for three days with CD3/CD28 Dynabeads in murine T cell medium. For the cell surface binding assay, prior to infection, cells were cooled (4°C, 30 min) to arrest cellular uptake. Cooled cells were treated with AAV6 or Ark313 containing a scCBh-GFP cassette at 1×10^5 vg/cell (1 h, 4°C) to promote viral binding but not uptake. Unbound virions were washed out with ice cold PBS three times, and viral and cellular DNA was extracted using an IBI genomic DNA extraction kit. Uptake was assayed using a similar stepwise process as for binding, except that after washing out unbound virions, cells were warmed with medium at 37°C and incubated in a 5% CO_2 incubator (37°C, 1 h) to facilitate uptake of bound virions. After incubation, cells were washed and trypsinized with 0.05% TrypLE Express (ThermoFisher Scientific #12605036) for 5 min to remove uninternalized virus, and viral and cellular DNA was extracted. qPCR analysis was performed on the DNA extracts for GFP to detect viral recombinant DNA, and for *Lamin-B1* to detect cellular DNA. The relative quantity of each amplicon was determined by comparison to a serial dilution of either vector plasmid or mouse genomic DNA of known concentration.

Assays for phosphoinositide phospholipase C GPI cleavage—To cleave GPI-anchored proteins, 1×10^5 activated C57BL6/J T cells in 100 μl murine T cell medium were pre-treated with bacterial phosphoinositide phospholipase C (PI-PLC; 1 U/ml; ThermoFisher Scientific #P6466) for 1 h at 37°C prior to assays for viral binding or transduction. Binding studies were carried out as described in the previous methods section. Transduction assays were performed at an MOI of 1×10^5 vg/cell for 48 h before flow cytometry analysis for GFP expression.

Nucleofection—After 24 h of T cell activation, CD3/CD28 Dynabeads were magnetically removed, and T cells were nucleofected in P3 buffer (Lonza #V4SP-3096) with ribonucleoprotein (RNP) using a 4D-Nucleofector 96-well unit (Lonza #AAF-1003S). An amount of RNP for one reaction was generated by incubating 60 pmol Cas9 protein (QB3 MacroLab) and 120 pmol sgRNA (Synthego) at 37°C. 2×10^6 cells were electroporated with RNP per well. Lonza program code DN-100 was used for murine T cells, and EH-115 was used for human T cells. After nucleofection, cells were diluted in culture medium and incubated (37°C, 5% CO_2). For making knock-ins, AAV was added to the culture between 30–60 min after nucleofection at the indicated MOI, and the culture was incubated overnight. The next day, the medium was exchanged for fresh T cell medium, and cells were expanded using standard culture conditions and maintained at a density of approximately 2×10^6 cells per ml.

Retroviral production and transduction—3.5×10^6 HEK293T cells were seeded in a 10-cm dish. Approximately 24 h later, the medium was replaced with 5 ml cDMEM, and cells were transfected with 7.5 μg pCL-ECO plasmid and 7.5 μg MSCV plasmid using Lipofectamine LTX with PLUS reagent (Invitrogen #15338030). The transfection mix was prepared in 3 ml Opti-MEM medium (Gibco #31985062) and incubated for at least 30 min at room temperature before being pipetted dropwise onto the cell culture. At 24 h after transfection, the medium was exchanged for 6 ml cDMEM collection medium. Retrovirus was harvested, sterile-filtered, and frozen for storage at 24 and at 48 h.

Transductions were performed on murine T cells at least 24 h after activation. 6-well plates were coated with 15 μg/ml retronectin (Takara # T100B) overnight at 4°C. The wells were gently rinsed with PBS prior to adding 3×10^6 activated murine T cells. Retrovirus was added to the cells to bring the total per-well volume to 2 ml, with 10 μg/ml polybrene. Cells were spinfected (2000×g, 30°C, 60 min) and then incubated overnight in a 37°C CO_2 incubator. The next day, the medium was exchanged for fresh T cell medium.

LL2-Luc2 cells were seeded and cultured for 24 h before transduction with retrovirus and 10 μg/ml polybrene, with overnight incubation. Transduced cells were selected with puromycin (2 μg/ml) for three days. Puromycin was subsequently maintained in the culture medium for these cells.

Genome-wide CRISPR/Cas9 screening—A genome-wide sgRNA knockout library targeting 18,424 genes (a total of 90,230 sgRNAs) in an MSCV plasmid was obtained from Addgene (#104861) and amplified following the instructions provided for maintaining library representation[29]. Viral packaging and transductions were performed using methods described in the previous methods section. The screen was performed with two technical replicates, each maintaining at least 500-fold coverage throughout the experimental procedure. For each replicate, 9×10^7 activated Cas9-expressing murine T cells from H11-Cas9 mice were transduced with the retroviral library by spinfection and incubated overnight. Transduction efficiencies of at least 50% were confirmed for each replicate by flow cytometry for BFP expression. The cells were cultured and expanded for 48 h before being re-activated using CD3/CD28 Dynabeads at a 1:1 ratio. At 24 h after re-activation (i.e., 96 h after the initial spinfection), 1.5×10^8 cells per replicate were transduced with

Ark313 scAAV-CAG-GFP at an MOI of 3×10^4. At 48 h after AAV transduction, cells were prepared for sorting by 7-AAD live-dead staining (eBioscience #00–6993-50), followed by fixation in 4% formaldehyde in PBS (15 min, 4°C) with cells at a concentration of 10^7 cells per ml. Fixed BFP-positive cells in FACS buffer were sorted in to four bins based on GFP expression; a total output of $>4.5 \times 10^7$ cells per replicate were sorted at the UCSF Parnassus Flow Cytometry Core (PFCC).

After sorting, genomic DNA was isolated as described previously[50], sgRNA barcodes were PCR-amplified using *Ex Taq* DNA polymerase (Clontech #RR001A) for 28 cycles, and amplicons were purified using SPRI beads. PCR primers were designed for Illumina sequencing with barcoded P7 primers. The barcode binding region was 5'-TTGTGGAAAGGACGAAACACCG-3' for the P5 adapter and 5'-CTAAAGCGCATGCTCCAGACTG-3' for the P7 adapter. Amplicon libraries were sequenced with Illumina NextSeq500 using the NextSeq 500/550 high output kit v2.5 (Illumina #20024906), with 500-fold coverage as the targeted depth of sequencing.

Analysis of FACS-based screen—Sequencing data were mapped to the reference library using MAGeCK *count* with the argument *--trim-5 22,23,24,25,26,28,29,30* to remove a staggered 5' adapter[51]. The resulting raw counts were input into a Bayesian hierarchical model called waterbear. The model treats each sgRNA from each replicate as a draw from a four-dimensional Dirichlet-multinomial distribution, with each dimension corresponding to a bin from cell sorting. Effects were modeled by a spike-and-slab approach, similar to Bayesian sparse linear mixed models[52]. During each MCMC sample, if a gene is included in the model, all of its sgRNAs are allowed to have correlated effect sizes conditionally independent given the overall gene-level effect size. If the gene is not included in the model, all of the guides are modeled to have an effect size of zero. The model was implemented in NIMBLE[53] and four chains were run, each with 10,000 burn-in samples and 10,000 additional samples that were kept for posterior summaries. We interpreted genes that had a posterior inclusion probability (PIP) > 0.9 to have an effect, and these high-PIP genes were used for gene ontology enrichment analysis[54]. Results are presented as a volcano plot. The x-axis is gene effect, where a negative value indicates enrichment in the GFP-low bins. The y-axis is -log10 (*lfsr*)[55], which refers to the error probability. A higher y-axis value indicates a lower error probability.

QUANTIFICATION AND STATISTICAL ANALYSIS

Statistical analyses were performed using GraphPad Prism9 (Dotmatics). All statistical details can be found in the figure legends. Results are presented as mean ± SEM, ns = not significant; $*p<0.05$; $**p<0.01$; $***p<0.001$; $****p<0.0001$.

Supplementary Material

Refer to Web version on PubMed Central for supplementary material.

ACKNOWLEDGMENTS

Declaration of Interests

REFERENCES

1. Sadelain M, Riviere I, and Riddell S. (2017). Therapeutic T cell engineering. Nature 545, 423–431. 10.1038/nature22395. [PubMed: 28541315]

2. June CH, O'Connor RS, Kawalekar OU, Ghassemi S, and Milone MC (2018). CAR T cell immunotherapy for human cancer. Science 359, 1361–1365. 10.1126/science.aar6711. [PubMed: 29567707]

3. June CH, and Sadelain M. (2018). Chimeric Antigen Receptor Therapy. N Engl J Med 379, 64–73. 10.1056/NEJMra1706169. [PubMed: 29972754]

4. Fraietta JA, Nobles CL, Sammons MA, Lundh S, Carty SA, Reich TJ, Cogdill AP, Morrissette JJD, DeNizio JE, Reddy S, et al. (2018). Disruption of TET2 promotes the therapeutic efficacy of CD19-targeted T cells. Nature 558, 307–312. 10.1038/s41586-018-0178-z. [PubMed: 29849141]

5. Shah NN., Qin H., Yates B., Su L., Shalabi H., Raffeld M., Ahlman MA., Stetler-Stevenson M., Yuan C., Guo S., et al. . (2019). Clonal expansion of CAR T cells harboring lentivector integration in the CBL gene following anti-CD22 CAR T-cell therapy. Blood Adv 3, 2317–2322. 10.1182/bloodadvances.2019000219. [PubMed: 31387880]

6. Sather BD, Romano Ibarra GS, Sommer K, Curinga G, Hale M, Khan IF, Singh S, Song Y, Gwiazda K, Sahni J, et al. (2015). Efficient modification of CCR5 in primary human hematopoietic cells using a megaTAL nuclease and AAV donor template. Sci Transl Med 7, 307ra156. 10.1126/scitranslmed.aac5530.

7. Eyquem J, Mansilla-Soto J, Giavridis T, van der Stegen SJ, Hamieh M, Cunanan KM, Odak A, Gonen M, and Sadelain M. (2017). Targeting a CAR to the TRAC locus with CRISPR/Cas9 enhances tumour rejection. Nature 543, 113–117. 10.1038/nature21405. [PubMed: 28225754]

8. Roth TL, Puig-Saus C, Yu R, Shifrut E, Carnevale J, Li PJ, Hiatt J, Saco J, Krystofinski P, Li H, et al. (2018). Reprogramming human T cell function and specificity with non-viral genome targeting. Nature 559, 405–409. 10.1038/s41586-018-0326-5. [PubMed: 29995861]

9. Muller TR, Jarosch S, Hammel M, Leube J, Grassmann S, Bernard B, Effenberger M, Andra I, Chaudhry MZ, Kauferle T, et al. (2021). Targeted T cell receptor gene editing provides predictable T cell product function for immunotherapy. Cell Rep Med 2, 100374. 10.1016/j.xcrm.2021.100374.

10. Schober K, Muller TR, Gokmen F, Grassmann S, Effenberger M, Poltorak M, Stemberger C, Schumann K, Roth TL, Marson A, and Busch DH (2019). Orthotopic replacement of T-cell receptor alpha- and beta-chains with preservation of near-physiological T-cell function. Nat Biomed Eng 3, 974–984. 10.1038/s41551-019-0409-0. [PubMed: 31182835]

11. Mansilla-Soto J, Eyquem J, Haubner S, Hamieh M, Feucht J, Paillon N, Zucchetti AE, Li Z, Sjostrand M, Lindenbergh PL, et al. (2022). HLA-independent T cell receptors for targeting tumors with low antigen density. Nat Med 28, 345–352. 10.1038/s41591-021-01621-1. [PubMed: 35027758]

12. Menger L., Sledzinska A., Bergerhoff K., Vargas FA., Smith J., Poirot L., Pule M., Hererro J., Peggs KS., and Quezada SA. (2016). TALEN-Mediated Inactivation of PD-1 in Tumor-Reactive Lymphocytes Promotes Intratumoral T-cell Persistence and Rejection of Established Tumors. Cancer Res 76, 2087–2093. 10.1158/0008-5472.CAN-15-3352. [PubMed: 27197251]

13. Seki A, and Rutz S. (2018). Optimized RNP transfection for highly efficient CRISPR/Cas9-mediated gene knockout in primary T cells. J Exp Med 215, 985–997. 10.1084/jem.20171626. [PubMed: 29436394]

14. Nguyen DN, Roth TL, Li PJ, Chen PA, Apathy R, Mamedov MR, Vo LT, Tobin VR, Goodman D, Shifrut E, et al. (2020). Polymer-stabilized Cas9 nanoparticles and modified repair templates increase genome editing efficiency. Nat Biotechnol 38, 44–49. 10.1038/s41587-019-0325-6. [PubMed: 31819258]

15. Kornete M, Marone R, and Jeker LT (2018). Highly Efficient and Versatile Plasmid-Based Gene Editing in Primary T Cells. J Immunol 200, 2489–2501. 10.4049/jimmunol.1701121. [PubMed: 29445007]

16. Madigan VJ, and Asokan A. (2016). Engineering AAV receptor footprints for gene therapy. Curr Opin Virol 18, 89–96. 10.1016/j.coviro.2016.05.001. [PubMed: 27262111]

17. Li C, and Samulski RJ (2020). Engineering adeno-associated virus vectors for gene therapy. Nat Rev Genet 21, 255–272. 10.1038/s41576-019-0205-4. [PubMed: 32042148]

18. Bryant DH, Bashir A, Sinai S, Jain NK, Ogden PJ, Riley PF, Church GM, Colwell LJ, and Kelsic ED (2021). Deep diversification of an AAV capsid protein by machine learning. Nat Biotechnol 39, 691–696. 10.1038/s41587-020-00793-4. [PubMed: 33574611]

19. Challis RC, Ravindra Kumar S, Chen X, Goertsen D, Coughlin GM, Hori AM, Chuapoco MR, Otis TS, Miles TF, and Gradinaru V. (2022). Adeno-Associated Virus Toolkit to Target Diverse Brain Cells. Annu Rev Neurosci. 10.1146/annurev-neuro-111020-100834.

20. Tabebordbar M, Lagerborg KA, Stanton A, King EM, Ye S, Tellez L, Krunnfusz A, Tavakoli S, Widrick JJ, Messemer KA, et al. (2021). Directed evolution of a family of AAV capsid variants enabling potent muscle-directed gene delivery across species. Cell 184, 4919–4938 e4922. 10.1016/j.cell.2021.08.028. [PubMed: 34506722]

21. Havlik LP, Das A, Mietzsch M, Oh DK, Ark J, McKenna R, Agbandje-McKenna M, and Asokan A. (2021). Receptor Switching in Newly Evolved Adeno-associated Viruses. J Virol 95, e0058721. 10.1128/JVI.00587-21.

22. Pomeroy EJ., Hunzeker JT., Kluesner MG., Lahr WS., Smeester BA., Crosby MR., Lonetree CL., Yamamoto K., Bendzick L., Miller JS., et al. . (2020). A Genetically Engineered Primary Human Natural Killer Cell Platform for Cancer Immunotherapy. Mol Ther 28, 52–63. 10.1016/j.ymthe.2019.10.009. [PubMed: 31704085]

23. Wang J, Exline CM, DeClercq JJ, Llewellyn GN, Hayward SB, Li PW, Shivak DA, Surosky RT, Gregory PD, Holmes MC, and Cannon PM (2015). Homology-driven genome editing in hematopoietic stem and progenitor cells using ZFN mRNA and AAV6 donors. Nat Biotechnol 33, 1256–1263. 10.1038/nbt.3408. [PubMed: 26551060]

24. Tse LV, Klinc KA, Madigan VJ, Castellanos Rivera RM, Wells LF, Havlik LP, Smith JK, Agbandje-McKenna M, and Asokan A. (2017). Structure-guided evolution of antigenically distinct adeno-associated virus variants for immune evasion. Proc Natl Acad Sci U S A 114, E4812–E4821. 10.1073/pnas.1704766114. [PubMed: 28559317]

25. Wu Z, Miller E, Agbandje-McKenna M, and Samulski RJ (2006). Alpha2,3 and alpha2,6 N-linked sialic acids facilitate efficient binding and transduction by adeno-associated virus types 1 and 6. J Virol 80, 9093–9103. 10.1128/JVI.00895-06. [PubMed: 16940521]

26. Wu Z, Asokan A, Grieger JC, Govindasamy L, Agbandje-McKenna M, and Samulski RJ (2006). Single amino acid changes can influence titer, heparin binding, and tissue tropism in different adeno-associated virus serotypes. J Virol 80, 11393–11397. 10.1128/JVI.01288-06. [PubMed: 16943302]

27. Huang LY, Patel A, Ng R, Miller EB, Halder S, McKenna R, Asokan A, and Agbandje-McKenna M. (2016). Characterization of the Adeno-Associated Virus 1 and 6 Sialic Acid Binding Site. J Virol 90, 5219–5230. 10.1128/JVI.00161-16. [PubMed: 26962225]

28. Pillay S, Meyer NL, Puschnik AS, Davulcu O, Diep J, Ishikawa Y, Jae LT, Wosen JE, Nagamine CM, Chapman MS, and Carette JE (2016). An essential receptor for adeno-associated virus infection. Nature 530, 108–112. 10.1038/nature16465. [PubMed: 26814968]

29. Henriksson J, Chen X, Gomes T, Ullah U, Meyer KB, Miragaia R, Duddy G, Pramanik J, Yusa K, Lahesmaa R, and Teichmann SA (2019). Genome-wide CRISPR Screens in T Helper Cells

Reveal Pervasive Crosstalk between Activation and Differentiation. Cell 176, 882–896 e818. 10.1016/j.cell.2018.11.044. [PubMed: 30639098]

30. Dudek AM., Zabaleta N., Zinn E., Pillay S., Zengel J., Porter C., Franceschini JS., Estelien R., Carette JE., Zhou GL., and Vandenberghe LH. (2020). GPR108 Is a Highly Conserved AAV Entry Factor. Mol Ther 28, 367–381. 10.1016/j.ymthe.2019.11.005. [PubMed: 31784416]

31. Devlin JJ, Weiss EH, Paulson M, and Flavell RA (1985). Duplicated gene pairs and alleles of class I genes in the Qa2 region of the murine major histocompatibility complex: a comparison. EMBO J 4, 3203–3207. 10.1002/j.1460-2075.1985.tb04066.x. [PubMed: 3004940]

32. Stroynowski I, Soloski M, Low MG, and Hood L. (1987). A single gene encodes soluble and membrane-bound forms of the major histocompatibility Qa-2 antigen: anchoring of the product by a phospholipid tail. Cell 50, 759–768. 10.1016/0092-8674(87)90334-5. [PubMed: 2441874]

33. da Silva IL, Montero-Montero L, Ferreira E, and Quintanilla M. (2018). New Insights Into the Role of Qa-2 and HLA-G Non-classical MHC-I Complexes in Malignancy. Front Immunol 9, 2894. 10.3389/fimmu.2018.02894. [PubMed: 30574154]

34. Stroynowski I, and Tabaczewski P. (1996). Multiple products of class Ib Qa-2 genes which ones are functional? Res Immunol 147, 290–301. 10.1016/0923-2494(96)89642-8. [PubMed: 8876057]

35. Das G, Gould DS, Augustine MM, Fragoso G, Sciutto E, Stroynowski I, Van Kaer L, Schust DJ, Ploegh H, and Janeway CA Jr. (2000). Qa-2-dependent selection of CD8alpha/alpha T cell receptor alpha/beta(+) cells in murine intestinal intraepithelial lymphocytes. J Exp Med 192, 1521–1528. 10.1084/jem.192.10.1521. [PubMed: 11085754]

36. Mellor AL, Antoniou J, and Robinson PJ (1985). Structure and expression of genes encoding murine Qa-2 class I antigens. Proc Natl Acad Sci U S A 82, 5920–5924. 10.1073/pnas.82.17.5920. [PubMed: 3862106]

37. Miller DG, Petek LM, and Russell DW (2004). Adeno-associated virus vectors integrate at chromosome breakage sites. Nat Genet 36, 767–773. 10.1038/ng1380. [PubMed: 15208627]

38. Honaker Y, Hubbard N, Xiang Y, Fisher L, Hagin D, Sommer K, Song Y, Yang SJ, Lopez C, Tappen T, et al. (2020). Gene editing to induce FOXP3 expression in human CD4(+) T cells leads to a stable regulatory phenotype and function. Sci Transl Med 12. 10.1126/scitranslmed.aay6422.

39. Madigan VJ, Tyson TO, Yuziuk JA, Pillai M, Moller-Tank S, and Asokan A. (2019). A CRISPR Screen Identifies the Cell Polarity Determinant Crumbs 3 as an Adeno-associated Virus Restriction Factor in Hepatocytes. J Virol 93. 10.1128/JVI.00943-19.

40. Comiskey M., Goldstein CY., De Fazio SR., Mammolenti M., Newmark JA., and Warner CM. (2003). Evidence that HLA-G is the functional homolog of mouse Qa-2, the Ped gene product. Hum Immunol 64, 999–1004. 10.1016/j.humimm.2003.08.352.

41. Heng TS, Painter MW, and Immunological Genome Project C. (2008). The Immunological Genome Project: networks of gene expression in immune cells. Nat Immunol 9, 1091–1094. 10.1038/ni1008-1091. [PubMed: 18800157]

42. Dietz S, Schwarz J, Velic A, Gonzalez-Menendez I, Quintanilla-Martinez L, Casadei N, Marme A, Poets CF, Gille C, and Kostlin-Gille N. (2021). Human Leucocyte Antigen G and Murine Qa-2 Are Critical for Myeloid Derived Suppressor Cell Expansion and Activation and for Successful Pregnancy Outcome. Front Immunol 12, 787468. 10.3389/fimmu.2021.787468.

43. Ran FA, Cong L, Yan WX, Scott DA, Gootenberg JS, Kriz AJ, Zetsche B, Shalem O, Wu X, Makarova KS, et al. (2015). In vivo genome editing using Staphylococcus aureus Cas9. Nature 520, 186–191. 10.1038/nature14299. [PubMed: 25830891]

44. Myers DR, Zikherman J, and Roose JP (2017). Tonic Signals: Why Do Lymphocytes Bother? Trends Immunol 38, 844–857. 10.1016/j.it.2017.06.010. [PubMed: 28754596]

45. Broz ML, Binnewies M, Boldajipour B, Nelson AE, Pollack JL, Erle DJ, Barczak A, Rosenblum MD, Daud A, Barber DL, et al. (2014). Dissecting the tumor myeloid compartment reveals rare activating antigen-presenting cells critical for T cell immunity. Cancer Cell 26, 638–652. 10.1016/j.ccell.2014.09.007. [PubMed: 25446897]

46. Yang Y, Kohler ME, Chien CD, Sauter CT, Jacoby E, Yan C, Hu Y, Wanhainen K, Qin H, and Fry TJ (2017). TCR engagement negatively affects CD8 but not CD4 CAR T cell expansion and leukemic clearance. Sci Transl Med 9. 10.1126/scitranslmed.aag1209.

47. Roth TL, Li PJ, Blaeschke F, Nies JF, Apathy R, Mowery C, Yu R, Nguyen MLT, Lee Y, Truong A, et al. (2020). Pooled Knockin Targeting for Genome Engineering of Cellular Immunotherapies. Cell 181, 728–744 e721. 10.1016/j.cell.2020.03.039. [PubMed: 32302591]

48. Gray SJ., Foti SB., Schwartz JW., Bachaboina L., Taylor-Blake B., Coleman J., Ehlers MD., Zylka MJ., McCown TJ., and Samulski RJ. (2011). Optimizing promoters for recombinant adeno-associated virus-mediated gene expression in the peripheral and central nervous system using self-complementary vectors. Hum Gene Ther 22, 1143–1153. 10.1089/hum.2010.245. [PubMed: 21476867]

49. Xiao X, Li J, and Samulski RJ (1998). Production of high-titer recombinant adeno-associated virus vectors in the absence of helper adenovirus. J Virol 72, 2224–2232. 10.1128/JVI.72.3.2224-2232.1998. [PubMed: 9499080]

50. Freimer JW, Shaked O, Naqvi S, Sinnott-Armstrong N, Kathiria A, Garrido CM, Chen AF, Cortez JT, Greenleaf WJ, Pritchard JK, and Marson A. (2022). Systematic discovery and perturbation of regulatory genes in human T cells reveals the architecture of immune networks. Nat Genet 54, 1133–1144. 10.1038/s41588-022-01106-y. [PubMed: 35817986]

51. Li W, Xu H, Xiao T, Cong L, Love MI, Zhang F, Irizarry RA, Liu JS, Brown M, and Liu XS (2014). MAGeCK enables robust identification of essential genes from genome-scale CRISPR/Cas9 knockout screens. Genome Biol 15, 554. 10.1186/s13059-014-0554-4. [PubMed: 25476604]

52. Zhou X, Carbonetto P, and Stephens M. (2013). Polygenic modeling with bayesian sparse linear mixed models. PLoS Genet 9, e1003264. 10.1371/journal.pgen.1003264.

53. Perry de Valpine DT, Christopher J. Paciorek, Clifford Anderson-Bergman, Duncan Temple Lang & Rastislav Bodik (2017). Programming With Models: Writing Statistical Algorithms for General Model Structures With NIMBLE, Journal of Computational and Graphical Statistics. Journal of Computational and Graphical Statistics 26, 403–413.

54. Raudvere U., Kolberg L., Kuzmin I., Arak T., Adler P., Peterson H., and Vil J. (2019). g:Profiler: a web server for functional enrichment analysis and conversions of gene lists (2019 update). Nucleic Acids Res 47, W191–W198. 10.1093/nar/gkz369. [PubMed: 31066453]

55. Stephens M. (2017). False discovery rates: a new deal. Biostatistics 18, 275–294. 10.1093/biostatistics/kxw041. [PubMed: 27756721]

HIGHLIGHTS

- A murine T cell–specific AAV variant, Ark313, is discovered through AAV6 evolution

- A genome-wide CRISPR screen identifies QA2 an essential factor for Ark313 transduction

- Ark313 enables efficient transgene delivery and targeting of large DNA payloads

- *Trac*-targeting of a CAR outperforms semi-random integration in a solid tumor model

Figure 1. Structure-guided evolution identifies an AAV capsid variant with murine T cell tropism

(A) Evolution of a pooled library of AAV6 capsid variants. The library was evolved for three cycles with CD3/CD28 bead–activated primary T cells from C57BL/6J mice and the parent and evolved libraries were analyzed by NGS.

(B) Sequencing analysis of the parental and evolved libraries. Bubble plots depict the enrichment of capsid mutants. Each bubble represents a unique amino acid sequence. Bubble size is proportional to enrichment in the evolved library.

(C) Sequence logo of the 7-mer sequence in the top 50 expressed capsids in the evolved library with more than 500-fold enrichment.

(D) Packaging yield of AAV6 (n=20) and Ark313 (n=11), presented as viral genomes per liter (vg/l) of medium used to produce virus. Viral genomes were quantified by qPCR.

(E) Number of viral genomes bound to the murine T cell surface following a 1 h incubation at 4°C to arrest cellular uptake, measured by qPCR. The bar graph depicts the mean ± SEM from four independent experiments.

(F) Percentage of internalized viral genomes after reactivation of membrane-bound AAV by a 1 h incubation at 37°C. The bar graph depicts the mean ± SEM from four independent experiments (n=4).

(G) scAAV-CBh-GFP was packaged into AAV6 and into Ark313. Transduction efficiencies were determined by flow cytometry at 48 hours after transduction.

(H) Flow cytometry analysis of EGFP expression following transduction of human T cells with AAV6 or Ark313 at the indicated MOIs. Left: fluorescence histograms. Right: MFI of transduced cells.

(I) Flow cytometry analysis of EGFP expression following transduction of murine T cells with AAV6 or Ark313 at the indicated MOIs. Left: fluorescence histograms. Right: MFI of transduced cells.

(D–F) Statistical significance was assessed using unpaired *t*-tests. ns = not significant; $*p<0.05$; $***p<0.001$.

Figure 2. Genome-wide CRISPR-Cas9 knockout screen identifies essential host factors for Ark313 infection

(A) Schematic of a genome-wide knockout screen to identify genes associated with Ark313 uptake and processing in primary murine T cells.

(B) Cas9-expressing C57BL/6J T cells were isolated from spleens, activated with CD3/CD28 beads, and transduced with the sgRNA library. Three days later, T cells were re-activated for 24 h and transduced with scAAV(Ark313)-CAG-GFP. At 48 h after Ark313 transduction, live BFP-positive cells were sorted into four bins based on GFP expression.

Genomic DNA was extracted from cells in each bin, and amplicon libraries were prepared and sequenced to determine sgRNA enrichment.

(C) The volcano plot depicts genes ranked by gene effect size (x-axis) and $-\log_{10}$ *lfsr* (y-axis) as determined by waterbear analysis. Genes with *lfsr* values <0.1 are highlighted in red.

(D) Top: distribution of $\log_2$ fold change (LFC) values of GFP-positive vs. GFP-negative cells for 90,230 guides in the library. Bottom: LFC for up to five sgRNAs targeting six depleted genes (red lines), overlaid on a gray gradient for the overall distribution. Values are the average of two technical replicates.

(E) Illustration of transmembrane MHC class Ib and GPI-anchored MHC class Ib.

(F) Arrayed validation of hits for the regulation of Ark313 infection. C57BL/6J T cells were nucleofected with RNPs targeting either *Aavr*, *Gpr108*, *B2m*, or *H2-Q7* for knockout, transduced with Ark313 scAAV-CAG-GFP at an MOI of 3×10^4, and analyzed by flow cytometry at 48 hours after transduction. Cells nucleofected with a SCR RNP were used as a negative control.

(G) Murine T cells were treated with PI/PLC to catalyze GPI cleavage, then transduced with scAAV-CBh-GFP in either AAV6 or Ark313. Surface-bound virus on murine T cells was measured (as viral genomes) by qPCR following a 1 h incubation at 4°C to arrest cellular uptake. Results are the mean ± SEM from four independent experiments (n=4).

(H) Murine T cells were treated with phosphatidylinositol-specific phospholipase C (PI/PLC) to catalyze GPI cleavage, then transduced with scAAV-CBh-GFP in either AAV6 or Ark313. GFP signal was analyzed by flow cytometry at 48 h to determine transduction. Results are the mean ± SEM from three independent experiments (n=3).

(I) BALB/cByJ T cells were transduced with gRV for expressing either mKate (gRV-mKate) or H2-Q7-P2A-mKate (gRV-H2-Q7). QA2 expression was measured by flow cytometry 5 days after transduction. WT BALB/cByJ and C57BL/6J T cells were used as controls. Transduced cells were gated as mKate[+].

(J) WT cells, gRV-mKate-transduced cells, and gRV-H2-Q7-transduced cells were transduced with scAAV-CBh-GFP in Ark313 at an MOI of 1×10^5 and analyzed by flow cytometry at 48 hours after transduction, gRV transduced cells were gated on mKate[+]. Left: representative histograms from one experiment. Right: results are the mean ± SEM from three mouse donors (n=3).

(G,H,J) Significance was assessed using a two-way ANOVA and Tukey's multiple comparison test. ns = not significant; ***p*<0.01; ****p*<0.001; *****p*<0.0001.
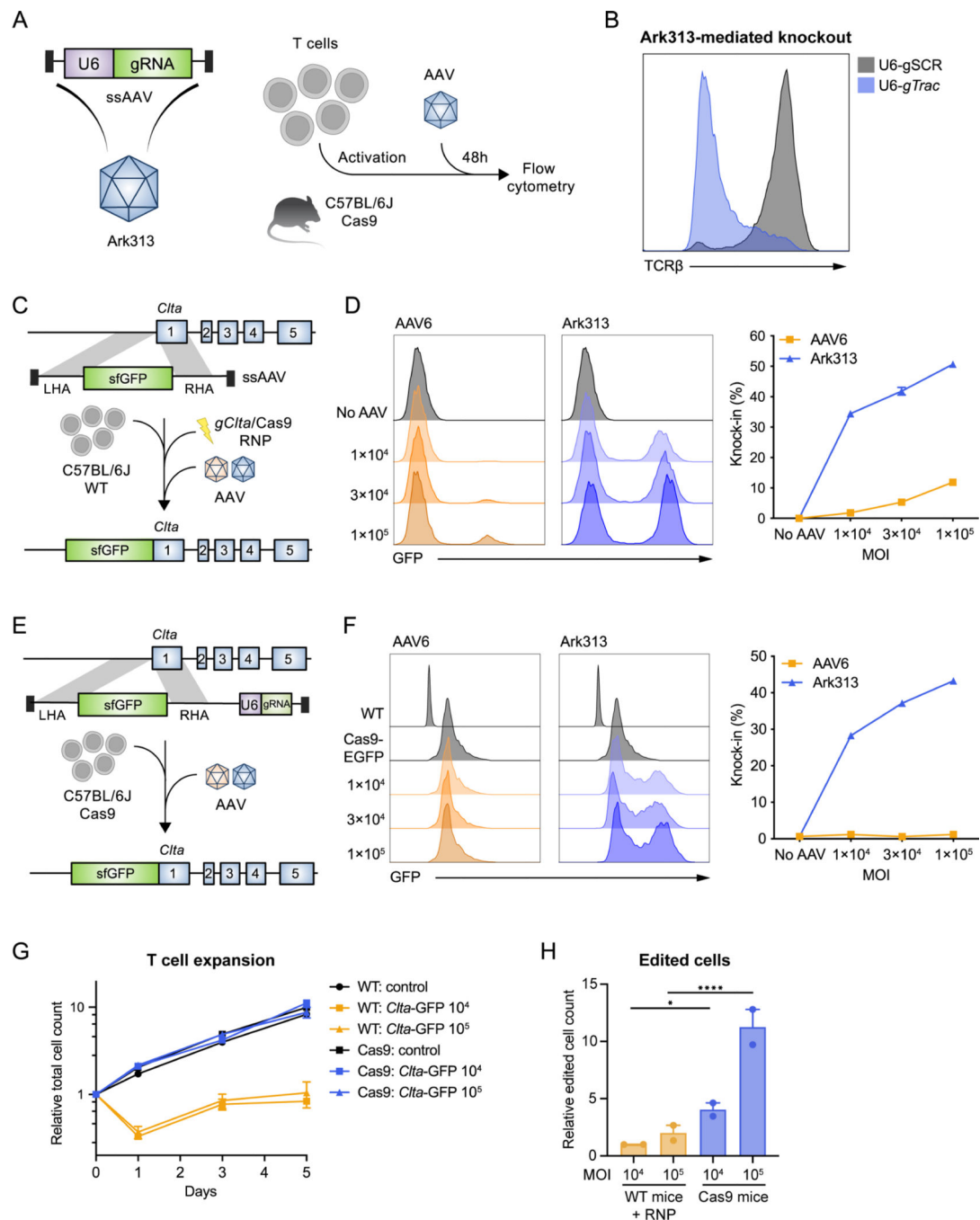
Figure 3. Ark313 enables efficient gene targeting in primary murine T cells

(A) Schematic of gene knockout by delivering an sgRNA to Cas9-expressing T cells using Ark313.

(B) Flow cytometry analysis of TCRβ expression in Cas9-expressing T cells following transduction with *Trac* sgRNA or scramble sgRNA using Ark313 at an MOI of 1×10^5.

(C) Integration of GFP HDRT at the *Clta* locus to generate a GFP-*Clta* fusion using Cas9-RNP nucleofection and AAV transduction.

(D) GFP integration was analyzed by flow cytometry. Knock-in efficiency was compared for AAV6 and Ark313 across a range of MOIs. Left: representative histograms from one experiment. Right: summary from three independent experiments (n=3).

(E) GFP integration at *Clta* in *Rosa26*-Cas9-EGFP T cells using single-AAV co-delivery of HDRT and sgRNA.

(F) Integration of GFP at *Clta* was analyzed by flow cytometry. Knock-in efficiency was compared between AAV6 and Ark313 across a range of MOIs. Left: representative histograms from one experiment. Right: summary from four independent experiments (n=4).

(G) Proliferation of WT T cells nucleofected with Cas9-RNP and transduced with AAV compared to AAV-transduced Cas9-expressing T cells. Results are the mean ± SEM from two mouse donors (n=2).

(H) Normalized yield of *Clta*-GFP edited cells after five days of expansion post-transduction, comparing Cas9-RNP-nucleofected and AAV-transduced WT cells to AAV-transduced Cas9-expressing T cells. Results are the mean ± SEM from two mouse donors (n=2). Significance was assessed using a one-way ANOVA and the Šidák multiple comparisons test. *p<0.05; ****p<0.0001.
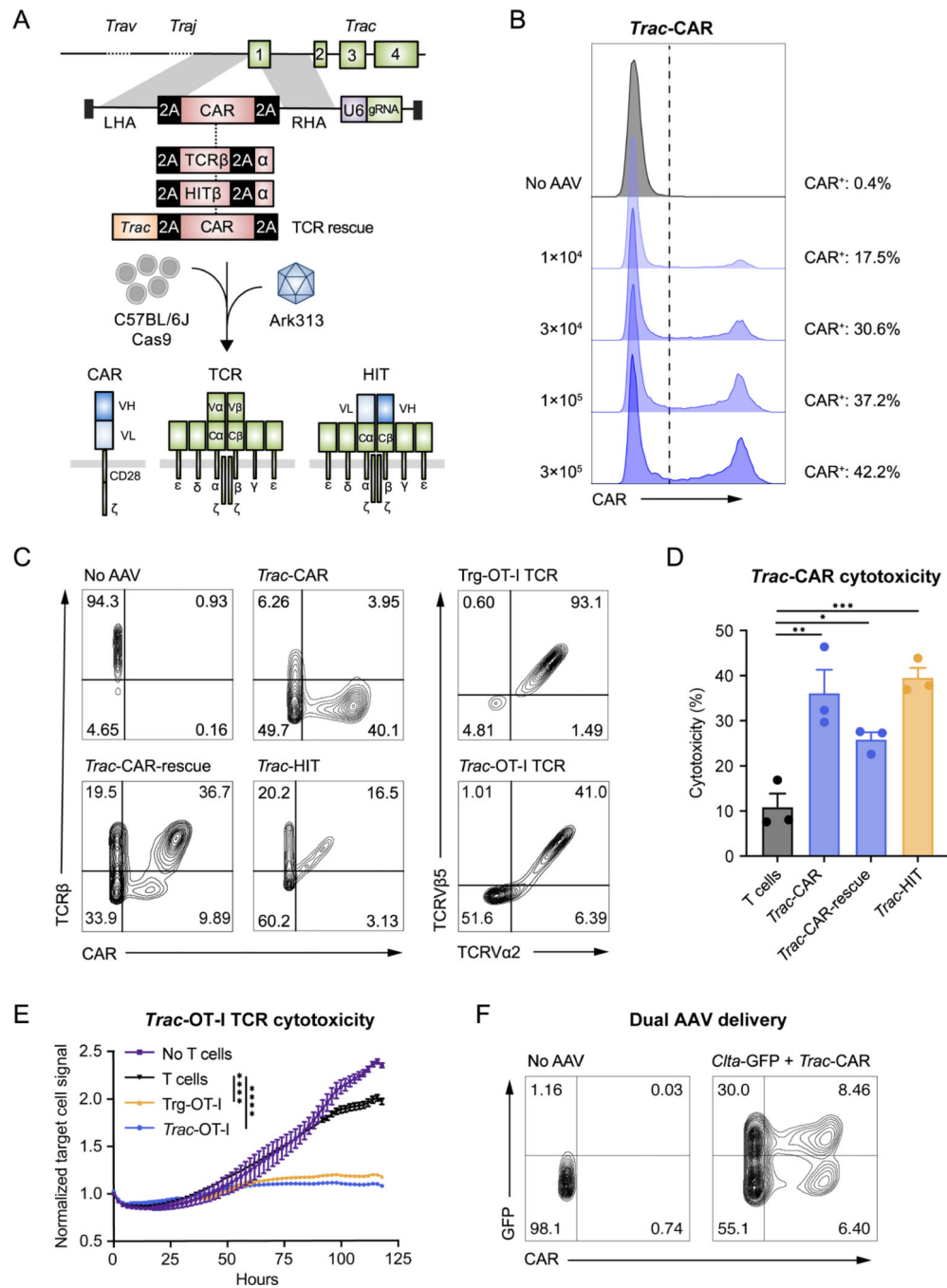
Figure 4. Targeting recombinant receptors to the *Trac* locus for experimental T cell immunology

(A) Schematic for targeted integration of a CAR, TCR, HIT, or CAR with TCR rescue at the *Trac* locus using co-delivery of HDRT and sgRNA in Ark313.

(B) Integration of a h19m28z CAR at the *Trac* locus by Ark313-mediated delivery to Cas9-expressing T cells. Left: flow cytometry analysis of CAR expression after transduction at different MOIs. Right: representative TCRβ and CAR flow cytometry plots for transduction with *Trac*-CAR Ark313.

(C) Left: representative TCRβ and CAR expression measured by flow cytometry after transduction with the indicated Ark313 HDRT at an MOI of 3×10^4. Edited cells express either CAR, CAR with rescued TCR expression, or HIT. Right: expression of *Trac*-targeted OT-I TCR T cells in comparison to T cells isolated from transgenic OT-I TCR mice.

(D) Cytotoxicity was determined based on the luciferase signal after a 24-hour co-culture of T cells with LL2 cells that express luciferase and hCD19. Results are the mean ± SEM from three technical replicates. Significance was assessed using one-way ANOVA and Dunnett's multiple comparisons test.

(E) Incucyte analysis of *Trac*-OT-I TCR T cells co-cultured with B78 cells that express mCherry and OVA. Results are the mean ± SEM from three technical replicates. Significance was assessed using a repeated-measures one-way ANOVA and Dunnett's multiple comparisons test.

(F) Efficacy of dual-gene targeting in murine T cells. GFP and CAR flow cytometry plots of Cas9-expressing T cells transduced with GFP-*Clta* and *Trac*-CAR Ark313 viruses at an MOI of 1×10^5 for each AAV.

(D,E) *$p<0.05$; **$p<0.01$; ***$p<0.001$; ****$p<0.0001$.
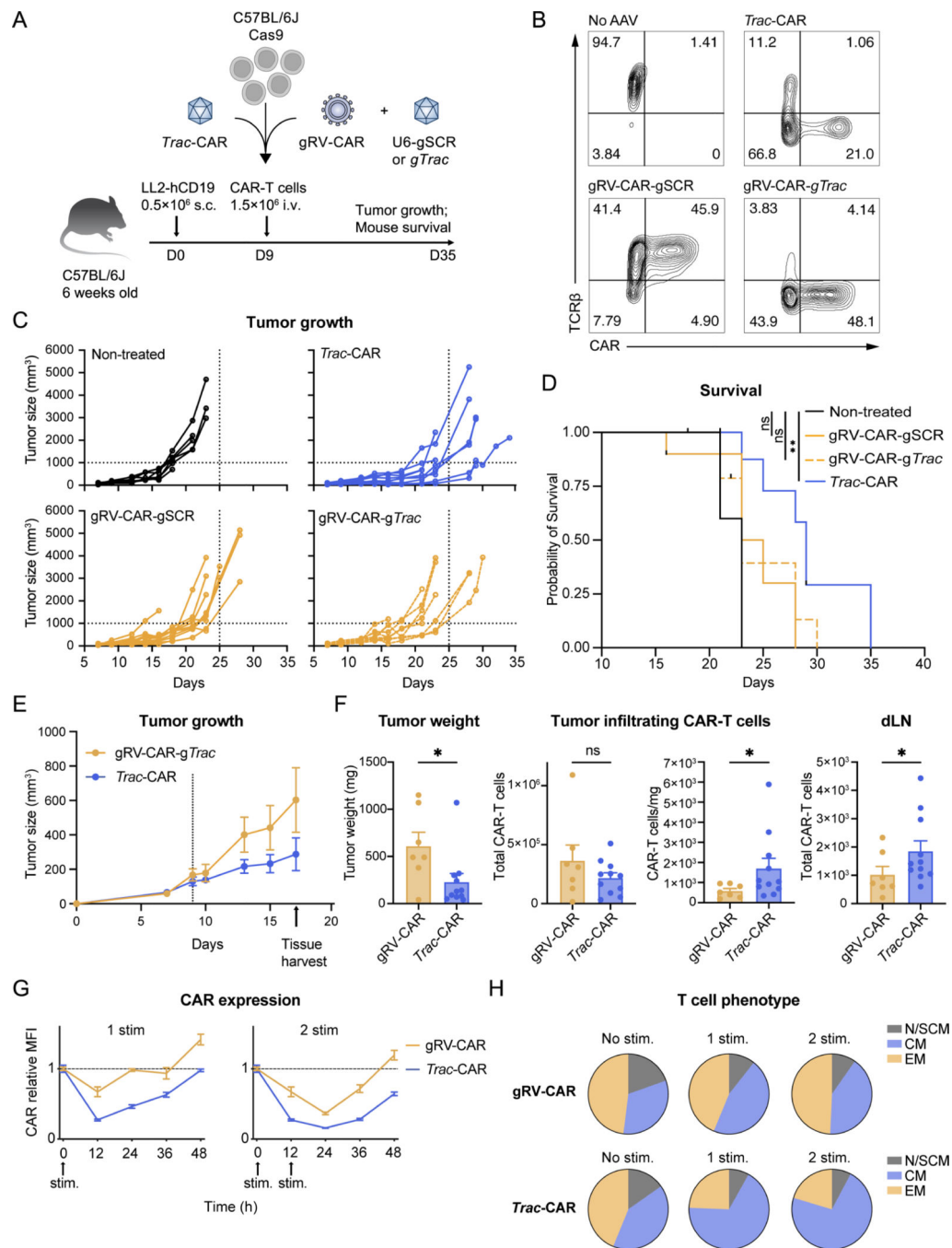
Figure 5. Targeting a CAR to the *Trac* locus using Ark313 enhances tumor control in an immunocompetent solid tumor mouse model

(A) Schematic of the syngeneic solid tumor model. hCD19-expressing LL2 cells were injected subcutaneously into C57BL/6J mice. The tumor-bearing mice were treated with either Ark313 *Trac*-CAR-T cells or gRV-CAR-T cells expressing the same h19m28z. The gRV-CAR-T cells were co-transduced with Ark313 expressing either a SCR sgRNA or *Trac*-targeting sgRNA to generate TCR+ and TCR− CAR-T cells, respectively. Mice were pre-treated with 100 mg/kg cyclophosphamide two days before T cell injection.

(B) Flow cytometry plots of TCRβ and CAR expression for engineered T cells using the indicated methods.

(C) Tumor growth in non-treated (n=6) mice and in mice treated with 1.5×10^6 *Trac*-CAR-T cells (n=9), gRV-CAR-gSCR T cells (n=10), or gRV-CAR-g*Trac* T cells (n=10).

(D) Kaplan-Meier survival analysis of mice injected with hCD19-expressing LL2 cells. Comparison of non-treated mice to mice injected with either *Trac*-CAR-T cells (n=9), gRV-CAR-gSCR T cells (n=10), or gRV-CAR-g*Trac* T cells (n=10). Significance was assessed using a log-rank (Mantel-Cox) test.

(E) Tumor growth in mice treated with 2×10^6 *Trac*-CAR-T cells (n=11) or gRV-CAR-g*Trac* T cells (n=7).

(F) Tumor and dLNs were isolated nine days after T cell injection. Tumors were weighed, and flow cytometry was conducted on the tumor and dLNs together. Results are the mean ± SEM. Significance were assessed using one-tailed Mann-Whitney tests.

(G) *Trac*-CAR-T cells and gRV-CAR-g*Trac* T cells underwent either one stimulation (0 h) or two stimulations (0 and 12 h) with LL2-hCD19 cells. CAR MFI was measured at 12 h intervals for 48 h. Results are the mean ± SEM from three technical replicates (n=3).

(H) T cell memory formation as determined by CD44 and CD62L expression at 48 h after either one or two stimulations with LL2-hCD19 cells. EM: CD44^{hi} CD62L^{lo}. CM: CD44^{hi} CD62L^{hi}. N/SCM: CD44^{lo} CD62^{hi}.

(D,F) ns = not significant; *$p<0.05$; **$p<0.01$.

Key resources table

REAGENT or RESOURCE	SOURCE	IDENTIFIER
Antibodies		
PE-Vio770 anti-mouse QA2	Miltenyi Biotec	#130-103-909
Vioblue anti-mouse QA2	Miltenyi Biotec	#130-103-905
Alexa Fluor 647 anti-mouse F(ab')$_2$	Jackson ImmunoResearch	#115-606-003
APC-Cy7 anti-mouse TCRβ	BD biosciences	#560656
BV421 anti-mouse TCRVα2	BioLegend	#127825
APC anti-mouse TCRβ5.1	BioLegend	#139506
BV421 anti-mouse CD90.1	BioLegend	#202529
BUV737 anti-human CD19	BD biosciences	#564303
BUV496 anti-human CD19	BD biosciences	#612938
BV711 anti-mouse CD8a	BD biosciences	#563046
BUV395 anti-mouse CD4	BD biosciences	#740208
BUV737 anti-mouse CD90.2	BD biosciences	#741702
Alexa Fluor 647 anti-mouse CD90.2	BioLegend	#105318
BV605 anti-mouse CD62L	BD biosciences	#563252
BUV737 anti-mouse CD44	BD biosciences	#612799
BUV605 anti-mouse B2M	BD biosciences	#745120
BV421 anti-mouse CD45.1	BioLegend	#110731
BUV395 anti-mouse CD45.2	BD biosciences	#564616
Bacterial and virus strains		
DH10B ElectroMax cells	Invitrogen	#18290015
NEB Stable Competent E.coli	NEB	#C3040I
AAV6 sc-CBh-GFP	This paper	N/A
AAV6 ss-CBA-GFP	This paper	N/A
Ark313 sc-CBh-GFP	This paper	N/A
Ark313 ssCBA-GFP	This paper	N/A
AAV6 sc-CAG-GFP	This paper	N/A
Ark313 sc-CAG-GFP	This paper	N/A
AAV6-Clta-GFP	This paper	N/A
Ark313-Clta-GFP	This paper	N/A
AAV6-U6/gClta-Clta-GFP	This paper	N/A
Ark313-U6/gClta-Clta-GFP	This paper	N/A
Ark313-Trac-h19m28z	This paper	N/A
Ark313-U6/gTrac-Trac-h19m28z	This paper	N/A
Ark313-U6/gTrac-Trac-h19m28z-P2A-Thy1.1	This paper	N/A
Ark313-U6/gTrac-Trac-HIT	This paper	N/A

REAGENT or RESOURCE	SOURCE	IDENTIFIER
Ark313-U6/gTrac-Trac-OT-I	This paper	N/A
Ark313-U6/gTrac-Trac-h19m28z-TCRrescue	This paper	N/A
gRV-h19m28z-P2A-Thy1.1	This paper	N/A
gRV-Puro-EFS-mKate	This paper	N/A
gRV-Puro-EFS-H2-Q7-P2A-mKate	This paper	N/A
Ark313-U6/gSCR	This paper	N/A
Ark313-U6/gTrac	This paper	N/A
gRV-GW-CRISPR-KO-BFP	This paper	N/A
Biological samples		
Chemicals, peptides, and recombinant proteins		
Zombie Violet	BioLegend	#423114
Puromycin	Gibco	#A1113803
GlutaMAX DMEM	Gibco	#10566024
RPMI 1640	Gibco	#11875093
Streptomycin	ThermoFisher Scientific	#15140122
Penicillin-streptomycin	ThermoFisher Scientific	#15140122
Sodium pyruvate	Gibco	#11360070
HEPES	Corning	#25-060-CI
β-mercaptoethanol	Gibco	#21985-023
MEM non-essential amino acids	Gibco	#11140050
Ghost Dye Red 780	Tonbo	#13-0865-T100
7-AAD	eBioscience	#00-6993-50
Propidium iodide	MilliporeSigma	#P4170
Normal mouse serum	MilliporeSigma	#NS03L
Polyethylenimine	Polysciences	#23966
Benzonase	Millipore Sigma	#70-664-3
OptiPrep	StemCell Technologies	#07820
DNaseI	NEB	#B0303S
Proteinase K	Qiagen	#1114886
SsoFast Eva Green Supermix	Bio-Rad	#1725201
Collagenase IV	Worthington	#LS004189
DNase I	Millipore Sigma	#10104159001
FBS	Corning	#35016CV
EDTA	Invitrogen	#15575020
Cyclophosphamide	Sigma Aldrich	#C07681G

REAGENT or RESOURCE	SOURCE	IDENTIFIER
ACK lysing buffer)	Quality biological	#118-156-101
Recombinant human IL-2	Peprotech	#200-02
X-VIVO 15 medium	Lonza	#BP04-744Q
Human serum	Gemini Bioproducts	#100-512
Recombinant human IL-7	Miltenyi Biotec	#130-095-367
Recombinant human IL-15	Miltenyi Biotec	#130-095-760
D-Luciferin	Goldbio	#LUCK-1G
TrypLE Express	ThermoFisher Scientific	#12605036
PI-PLC	ThermoFisher Scientific	#P6466
Cas9 protein	QB3 MacroLab	Cas9-NLS purified protein (2.5 mg)
Lipofectamine LTX with PLUS reagent	Invitrogen	#15338030
Opti-MEM medium	Gibco	#31985062
Retronectin	Takara	#T100B
Polybrene	Millipore Sigma	#TR-1003-G
Ex Taq DNA polymerase	Clontech	#RR001A
BsiWI-HF	NEB	#R3553S
SbfI-HF	NEB	#R3642S
T4 DNA ligase	NEB	#M0202S
Q5 polymerase	NEB	#M0492S
M3814 (Nedisertib)	ChemieTek	#CT-M3814
Critical commercial assays		
CountBright Absolute Counting Beads	Invitrogen	#C36950
IBI genomic DNA extraction kit	IBI Scientific	#IB47280
ZymoPURE II plasmid maxiprep kit	Zymo Research	#D4203
EasySep mouse T cell isolation kit	STEMCELL Technologies	#19851
Dynabeads Mouse T-Expander CD3/CD28	Gibco	#11452D
EasySep Human T cell isolation kit	STEMCELL Technologies	#17951
Dynabeads Human T-Activator CD3/CD28	ThermoFisher	#11131D
NextSeq 500/550 high output kit v2.5	Illumina	#20024906
NovaSeq 6000 S4 Reagent Kit v1.5 (300 cycles)	Illumina	#20028312
Deposited data		
AAV6 evolution sequencing data	This paper	GEO: GSE216427
Genome-wide KO screen for Ark313 essential genes	This paper	GEO: GSE216819
Experimental models: Cell lines		

REAGENT or RESOURCE	SOURCE	IDENTIFIER
HEK293T	ATCC	#CRL-3216
LL/2-Luc2	ATCC	#CRL-1642-LUC2
OVA.mCherry.B78	Krummel lab (UCSF)	N/A
721.221 human HLA-negative B cell line	Millipore Sigma	#SCC275
HLA-G-expressing 721.221	Lanier lab (UCSF)	N/A
Experimental models: Organisms/strains		
Mouse: C57BL/6J	The Jackson Laboratory	#000664
Mouse: BALB/cJ	The Jackson Laboratory	#000651
Mouse: BALB/cByJ	The Jackson Laboratory	#001026
Mouse: H11-Cas9 on C57BL/6J	The Jackson Laboratory	#028239
Mouse: Rosa26-Cas9 knock-in on C57BL/6J	The Jackson Laboratory	#026179
Mouse: C57BL/6J-Ptprcem6Lutzy/J	The Jackson Laboratory	#033076
Mouse: NOD	Qizhi Tang lab (UCSF)	N/A
Human: Leukopak	STEMCELL Technologies	#70500.1
Oligonucleotides		
Primers for AAV titration, see Table S1	This paper	N/A
Primers for Genomic DNA KI validation, see Table S1	This paper	N/A
Primers for Genomic DNA indel frequency, see Table S1	This paper	N/A
Primers for Capsid library, see Table S1	This paper	N/A
Primers for Illumina seq Capsid library, see Table S1	This paper	N/A
Primers for Illumina seq KO screen, see Table S1	This paper	N/A
Primers for Binding/Uptake, see Table S1	This paper	N/A
gRNA sequences, see Table S1	This paper	N/A
Homolgy arms for KI, see Table S1	This paper	N/A
Recombinant DNA		
scAAV-CBh-GFP	Gray et al.[48]	N/A
ssAAV-CBA-GFP	This paper	N/A
scAAV-CAG-GFP	Addgene	#83279
MSCV-Puro-EFS:GFP	Addgene	#68484
pAAV-Clta-GFP	This paper	N/A
pAAV-U6/gClta-Clta-GFP	This paper	N/A
pAAV-Trac-h19m28z	This paper	N/A
pAAV-U6/gTrac-Trac-h19m28z	This paper	N/A
pAAV-U6/gTrac-Trac-h19m28z-P2A-Thy1.1	This paper	N/A
pAAV-U6/gTrac-Trac-HIT	This paper	N/A
pAAV-U6/gTrac-Trac-OT-I	This paper	N/A

REAGENT or RESOURCE	SOURCE	IDENTIFIER
pAAV-U6/gTrac-Trac-h19m28z-TCRrescue	This paper	N/A
MSCV-h19m28z-P2A-Thy1.1	This paper	N/A
MSCV-Puro-EFS-mKate	This paper	N/A
MSCV-Puro-EFS-H2-Q7-P2A-mKate	This paper	N/A
pAAV-U6/gSCR	This paper	N/A
pAAV-U6/gTrac	This paper	N/A
pHelper	This paper	N/A
pArk313	This paper	N/A
pArk6	This paper	N/A
pITR2-Rep2-dead(GFP)Cap6	This paper	N/A
pITR2-Rep2-STOPSTOPSTOPCap6	This paper	N/A
pXX680	Xiao et al.[49]	N/A
Retroviral Mouse Genome-wide CRISPR Knockout Library (Teichmann)	Addgene	#104861
Software and algorithms		
PSSMSearch	http://slim.icr.ac.uk/pssmsearch/	N/A
FlowJo v10.8.1	BD	N/A
Prism9	GraphPad by Dotmatics	N/A
Perl Script to analyze AAV library	Tse et al.[24]	N/A
Waterbear analysis for GW KO screen	DOI: 10.5281/zenodo.7349142	N/A
Other		

Author Manuscript

Author Manuscript

Author Manuscript

Author Manuscript